⑥ TUNNEL WALL INTERFERENCE FOR BODIES OF REVOLUTION
IN NON-STEADY MOTION,

⑩ William R./Hall

⑨ Master's thesis,

⑪ 31 Aug 73

⑫ 107p.

⑭ Technical Memorandum
File No. TM-73-224
August 31, 1973
⑮ Contract No. N00017-73-C-1418

Copy No. 5

The Pennsylvania State University
Institute for Science and Engineering
APPLIED RESEARCH LABORATORY
University Park, Pennsylvania

NAVY DEPARTMENT

NAVAL ORDNANCE SYSTEMS COMMAND

1473

391007

## ACKNOWLEDGEMENTS

## ABSTRACT

This thesis considers the problem of determining the effects of tunnel wall interference on the measured values of the stability derivatives for axisymmetric bodies. The tunnel wall interference corrections developed apply equally well to both subsonic wind tunnel or water tunnel testing in tunnels with circular test sections.

A linearized slender body theory is developed which can be used to predict corrections for:

(1) the static lift and pitching moment derivatives, $C_{L_\alpha}$ and $C_{M_\alpha}$

(2) the rotary damping derivatives, $C_{L_q}$ and $C_{M_q}$

(3) the "Add Mass" derivatives, $C_{L_{\dot\alpha}}$ and $C_{M_{\dot\alpha}}$ and

(4) the "Accession-to-Inertia" derivatives $C_{L_{\dot q}}$ and $C_{M_{\dot q}}$.

Limited evaluation of the developed theory is presented in the form of static pitching moment tests of three ellipsoids-of-revolution. In addition, comparison is made with two alternative theories developed by Peirce[1] and Goodman[2].

TABLE OF CONTENTS

# TABLE OF CONTENTS

# LIST OF TABLES

LIST OF FIGURES

## LIST OF FIGURES

## LIST OF SYMBOLS

$d_M$      model diameter as function of $x$

$d_T$      tunnel test section diameter, possibly a function of $x$

$C_{L_\alpha}$      static lift coefficient curve slope, per degree

$C_{M_\alpha}$      static pitching moment coefficient curve slope, per degree

$C_{L_q}$      lift rotary damping stability derivative

$C_{M_q}$      pitching moment rotary damping stability derivative

$C_{L_{\dot\alpha}}$      "Add-Mass" acceleration stability derivative, lift

$C_{M_{\dot\alpha}}$      "Add-Mass" acceleration stability derivative, moment

$C_{L_{\dot q}}$      "Accession-to-Inertia" acceleration stability derivative, lift

$C_{M_{\dot q}}$      "Accession-to-Inertia" acceleration stability derivative, moment

$U_x$      local velocity parallel to the body x-axis, at the body surface

$U$      free-stream velocity parallel to body x-axis

$V$      resultant velocity

$k$      reduced frequency, $\dfrac{\omega \ell}{U}$

$\ell$      overall body length

$f$      fineness ratio, $\ell/d$

$d$      maximum model diameter

$Re$      Reynolds number, $\dfrac{U\ell}{\nu}$

$S$      $\dfrac{\pi}{4} d_M^2$ , body cross-sectional area, function of $x$

## LIST OF SYMBOLS

$r$      radial coordinate, Figures 3 and 4

$x$      axial coordinate, Figure 3

$t$      time

$b$      body center of rotation, Figure 3

$q$      angular velocity, $\dot{\theta}_1$

$\dot{h}$      body plunging velocity, $q = 0$

$\dot{Z}_o$      total cross flow velocity in the $r\theta$ plane, Equation (9)

$R$      tunnel test section radius, function of $x$

$a$      local model radius, function of $x$

$\Delta P_a$      local pressure at the body periphery

$L$      total body lift

$M$      total body pitching moment

$C_p$      static wall pressure coefficient, $C_p = \dfrac{P - P_o}{1/2\rho U^2}$

$R_o$      tunnel test section radius where $C_p = 0$

$C'_p$      static wall pressure gradient, $\dfrac{dC_p}{dx}$

$C_L$      lift coefficient, Appendix A

$C_M$      pitching moment coefficient, Appendix A

$V$      body volume

$S_M$      maximum body cross-sectional area, $S_M = \dfrac{\pi d^2}{4}$

$K$      calibration constants for torque cell, pressure transducers, etc.

## LIST OF SYMBOLS

| | |
|---|---|
| $\nu$ | kinematic viscosity |
| $\phi$ | velocity potential |
| $\theta$ | aximuth angle, Figure 3 and 4 |
| $\theta_1$ | body pitch angle |
| $\mu$ | doublet strength, function of x |
| $\alpha$ | body angle-of-attack |
| $\rho$ | density |
| $\gamma$ | prismatic coefficient, $\dfrac{4\,V}{\pi_d{}^2 \ell}$ |
| $\omega$ | circular frequency |

## Subscripts

| | |
|---|---|
| FS | free-stream or unrestricted medium cases |
| IT | in-tunnel or in-tube cases |
| $(\ )_v$ | subscript v indicates differentiation with respect to v, where $v = x, r, \theta, \alpha, \dot{\alpha}, q,$ or $\dot{q}$ |

## Superscripts

| | |
|---|---|
| $(\ )'$ | differentiation with respect to x |
| $(\dot{\ })$ | differentiation with respect to time, t |
| $(\bar{\ })$ | overbar indicates non-dimensional quantity, see Appendix A |

CHAPTER I

INTRODUCTION

## Origin and Statement of the Problem

The motion of a body through a fluid gives rise to forces and
moments which are functionally dependent on the body velocities,
accelerations and control angles. For large changes in the velocities
and accelerations, these body forces and moments are related to the
body motion in a non-linear manner. Classically, in order to develop
mathematical expressions relating these *forces to the body motions,* a
Taylor series expansion in the body velocities, accelerations and
control angles is made. Experience has shown, for the motion of
slender bodies a linear Taylor series expansion in these variables
is adequate to describe small motions of the body from an equilibrium
condition. Thus, a typical aerodynamic force, A, may be written as

$$A = A_o + A_\alpha \, \alpha + A_{\dot\alpha} \, \dot\alpha + \ldots A_q \, q \qquad (1)$$

where $A_\alpha = \left(\dfrac{\partial A}{\partial \alpha}\right)_o$ .

The subscript zero indicates that the expression is to be evaluated
at the equilibrium condition. The proportionality constants, such as
$A_\alpha$, are called the stability derivatives. A valid Taylor series
expansion of Equation (1) requires the forces and moments to be

proportional to the instanteous values of the body velocities and accelerations. Thus, the stability derivatives are constants. Etkin[3] has shown that the derivatives are actually time dependent but converge to a constant value very rapidly. This implies that the stability derivative concept is valid except during the very beginning of the body motion.

The techniques used for experimentally determining the stability derivatives of a hydrodynamic body are quite valid. The techniques include static wind tunnel tests, rotating-arm tests[4], free flight trajectory studies[5],[6], and forced-oscillation tests[7],[8],[9],[10]. Tests in this last category can be conducted in the 48.0-inch diameter water tunnel[11] operated by the Applied Research Laboratory (ARL) of The Pennsylvania State University using a Planar Motion Mechanism[12]. The Planar Motion Mechanism incorporates in one device of the forced-oscillation type the means for experimentally determining all the stability derivatives of a hydrodynamic body. By forcing the body to follow a known sinusoidal path, the velocity and acceleration-dependent stability derivatives may be related to measured dynamic forces and moments. The development of the techniques required for determining stability derivatives with a Planar Motion Mechanism at the Applied Research Laboratory was accomplished through testing of the small basic finner missile model shown in Figure 1. A comparison of stability derivatives obtained with this model and similar data[13] from other sources is given by Table 1. In these tests, a small basic finner missile with a model-to-tunnel diameter ratio of 0.104 was used to
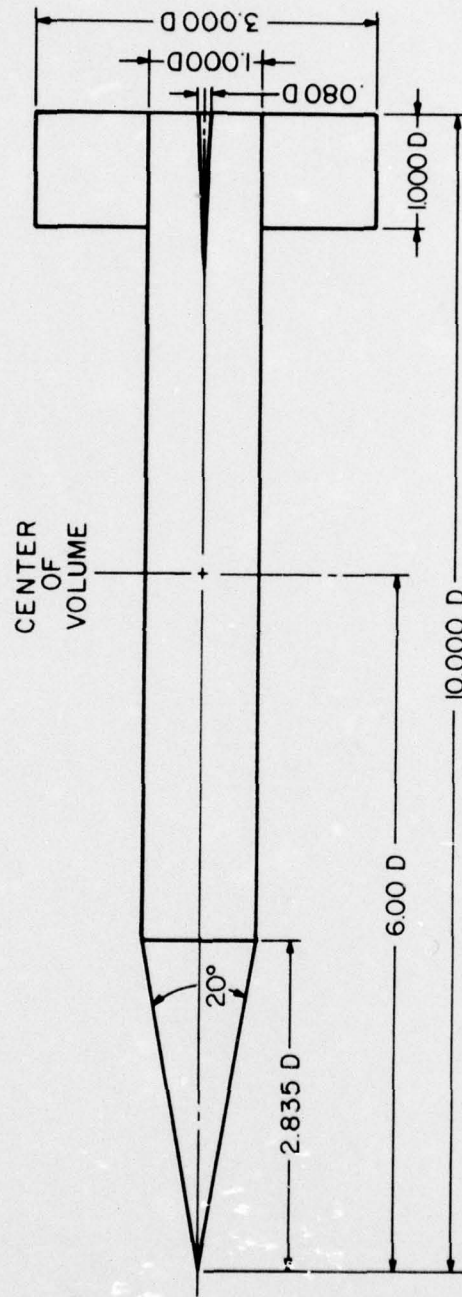
Figure 1  Sketch of the Basic Finner Missile Configuration

## TABLE 1

### COLLECTED BASIC FINNER MISSILE STABILITY DERIVATIVES

| ORIGINAL SOURCE[13] | STABILITY DERIVATIVES | | | | | |
|---|---|---|---|---|---|---|
| | $C_{L_\alpha}$ | $C_{M_\alpha}$ | $C_{L_\alpha}$ | $C_{L_q}$ | $C_{M_q}$ | $C_{L_q}$ |
| 1. Natl. Bureau of Stds. | | | | | | |
|   a. 4.0 in. dia. model | -0.0395 | -0.0195 | ------- | ------- | -0.0059 | ------- |
|   b. 2.0 in. dia. model | -0.1100 | -0.0205 | ------- | ------- | -0.0075 | ------- |
| 2. California Inst. of Tech. | | | | | | |
|   a. Angular Balance | -0.1107 | -0.0251 | ------- | -0.0409 | -0.0138 | -0.00079 |
|   b. Translat'l Balance | -0.1060 | ------- | -0.0134 | ------- | ------- | ------- |
|   c. Static Tests | -0.0997 | -0.0243 | ------- | ------- | ------- | ------- |
| 3. NSRDC PMM (2 ft.dia.model) | | | | | | |
|   a. Static Tests | -0.1054 | -0.0218 | ------- | ------- | ------- | ------- |
|   b. Dynamic Tests | ------- | ------- | -0.0108 | -0.0329 | -0.0107 | -0.00119 |
| 4. U. S. Naval Proving Grnd. Trajectory Analysis | -0.1147 | -0.0248 | ------- | -0.0304 | -0.0101 | ------- |
| 5. Theoretical Predictions | -0.1076 | -0.0224 | -0.0149 | -0.0357 | -0.0118 | -0.00094 |
| 6. ARL PMM (5 in.dia.model) | | | | | | |
|   a. Static Tests | -0.107 | -0.0248 | ------- | ------- | ------- | ------- |
|   b. Dynamic Tests | -0.123 | -0.0265 | -0.0125 | -0.0436 | -0.0142 | -0.00081 |

avoid tunnel wall interference. However, for typical models with large
model-to-tunnel diameter ratios, a question remains as to the extent
of the tunnel wall interference on the various stability derivatives.
Until such time as the extent of the tunnel wall interference on the
various stability derivatives as a function of model-to-tunnel diameter
ratio is resolved, the experimental stability derivative data obtained
for these models from tests with the planar motion mechanism are
suspect. Obviously, the conditions under which a model is tested in
a water or wind tunnel are not the same as those in an unrestricted
medium. A longitudinal static pressure gradient is usually present in
the test section. In addition to the tunnel walls, model supports,
local variations in flow velocity and angularity, and tunnel blockage
frequently result in extraneous interference forces for which the
experimental data must be corrected. In the past, much work has been
done to correct experimental data for flow angularity, local velocity
variations, tunnel blockage, and support interference and several
references[14] indicating common practices are available for the purpose.
In the case of the tunnel walls, the walls constrain the flow around
the body resulting in unwanted interference velocities not present in
the unrestricted medium. The extent of these unwanted velocities is
functionally dependent on the model-to-tunnel diamter ratio and the
body geometry. Since these unwanted velocities can produce extraneous
forces and moments characterized by errors in the measured stability
derivatives, some form of correction must be applied to the
experimental data.

This thesis explores both theoretically and experimentally the question of tunnel wall interference. The theoretical phase of this work attempts to develop a relatively simple theory for correcting the experimental stability derivatives of a general axisymmetric body for tunnel wall interference effects based on slender body theory. The general body shape implies that the body radius need not be an exact mathematical function, but rather the body radius as a function of axial position may be specified by a numerical tabulation. The tunnel wall interference corrections are presented in the form of multiplicative factors which may readily be applied to experimental test results. These tunnel wall interference corrections are defined as the ratio of in-tunnel to free stream stability derivatives. Corrections are indicated for:

1) the static lift and pitching moment derivatives, $C_{L_\alpha}$ and $C_{M_\alpha}$;

2) the rotary damping derivatives, $C_{L_q}$ and $C_{M_q}$;

3) the "Add Mass" derivatives, $C_{L_{\dot\alpha}}$ and $C_{M_{\dot\alpha}}$; and

4) the "Accession-to Inertia" derivatives, $C_{L_{\dot q}}$ and $C_{M_{\dot q}}$.

In the experimental phase, a limited experimental verification of the developed theory is presented in the form of wind tunnel tests of several ellipsoids-of-revolution. The ellipsoids-of-revolution were chosen on the basis of earlier works by Peirce[1] and Goodman[2] which provide some basis for comparison. Also, the ellipsoids-of-revolution permit exact formulation of the various stability

derivative integrands which may be compared with numerically specified integrands of the kind required if the developed theory to be applied to a general axisymmetric body.

## Previous Investigations

Much of the early work concerning tunnel wall interference for axisymmetric bodies was stimulated by the airship development efforts prior to 1936. Prime examples of this work are the papers of Munk[15], Abbott[16], Freeman[17] and Upson, et al[18]. Peirce indicates that most of the previous theoretical work on tunnel wall interference was done prior to 1933, while interest in the experimental determination of the aerodynamic characteristics of airships declined about 1936. This decline was spurred by the airship disasters of the mid-thirties and the rapid progress in airplane design. Even so, the bulk of this early work[19] on tunnel interference was concerned with blockage effects and increases in measured body drag due to the static pressure gradient in the tunnel created by the growth of the tunnel wall boundary layer. Also, in the majority of the experimental work on air-ships, the model-to-tunnel diameter ratio was 0.143 or less and most of the testing was performed in open-jet tunnels. Peirce indicates that the magnitude of the drag interference correction for an open-jet tunnel is approximately 75 percent that of a closed-section tunnel. Therefore, tunnel wall drag interference was small, and completely ignored by most investigators[16].

The advent of the guided missile, supersonic airplane, nuclear submarine, and high-speed torpedo, which are all essentially axisymmetric bodies incorporating very low aspect ratio wings, has resulted in further interest in the hydrodynamic characteristics of such bodies. Since experimental testing of such bodies is desirable, there has also been a resurgence of interest in the tunnel wall interference problem for them. Further impetus for research in these tunnel interference problems may be found in the development of high speed tube transportation systems, where the aerodynamic forces experienced by the body in the tube may be an order of magnitude greater than predicted from unrestricted medium data[2].

A literature search[20] prepared by NASA covering the period 1962 to 1972 has indicated that most research concerning aerodynamic characteristics of an axisymmetric body in a tunnel has been concerned with correcting the body drag for the static pressure grandient of the tunnel. Two notable exceptions are papers by Peirce and Goodman.

Peirce conducted a theoretical and experimental investigation of tunnel interference aimed at extending the capabilities of the ARL 48-inch diameter water tunnel. This tunnel was originally designed to study the problems of wake-operating propellers. Lehman states that for mechanical reasons such propellers must be at least 5 inches in diameter. For model submarine testing, propellers are approximately 7.5 inches in diameter and model body diameters are of the order of 16 inches. In testing such models in this tunnel, it can be expected that the tunnel wall interference, both to drag and to the stability

derivatives, may be significant. Indeed, during the initial testing of submarine models at ARL, it was discovered that existing methods of correcting for tunnel interference were inadequate.

For correcting drag, Peirce examined two approaches to the tunnel wall interference problem. One approach forces the flow around the body to conform to the stream pattern in an unrestricted medium by means of a flow correcting tunnel liner; the second considers further correction factors applied to the tunnel data. Due to the large corrections indicated, the latter alternative was quickly discarded. Subsequent testing of submarine models has verified that the flow correcting liner is quite useful in providing the correct operating environment for the wake-operating submarine propeller. That is, the liner supplies the correct pressure distribution along the body resulting in the proper boundary layer growth on the body. In addition, Peirce examined the effect of tunnel liner manufacturing deviations on body drag measurements and wall interference on the body pitching moment derivative, $C_{M_\alpha}$.

Following the slender body approach of Sprieter[21], Peirce predicts a maximum pitching moment derivative correction of

$$
\left( \frac{C_{M_{\alpha_{IT}}}}{C_{M_{\alpha_{FS}}}} \right)_{max} = \frac{1 + (d_M/d_T)^2_{max}}{\left[ 1 - (d_M/d_T)^2_{max} \right]^2} \quad , \tag{2}
$$

based on the maximum model-to-tunnel diameter ratio, $(d_M/d_T)_{max}$.
Subsequent experimental verification of Equation (2) shows agreement to
within 3 percent of predicted theoretical values. However, this maximum
correction factor ignores body geometric details and further refinement
may be useful. In any case, the pitching moment data of this reference
appears to be the only experimental tunnel wall correction data available.
Independent substantiation of these data constitutes part of the
experimental phases of this thesis. Also, Peirce's application of
slender body theory is reasonable, and by applying the techniques
suggested by Ribner[22], it may be extended to indicate corrections
for all the stability derivatives.

In conjunction with studies of a high speed tube transportation
system, Goodman assumes potential flow and formulates the expression
for the aerodynamic characteristics of a slender body traveling in a
tube. This is accomplished by following the perturbation techniques
suggested by Hoffman and Platzer[23] for obtaining the aerodynamic
characteristics of a slender body oscillating in supersonic flow. This
perturbation technique represents a refinement of classical slender
body theory[15],[21] permitting inclusion of transverse body forces
other than those produced by the cross-flow velocity. Generation of the
tunnel wall interference corrections by Goodman's method requires
solution of the Neumann problem for the axisymmetric flow past a body-
of-revolution in a tunnel and in an unrestricted medium. Goodman
obtains a simple expression for the required axial and radial velocity
components on the body surface by assuming a line source of variable
strength along the body centerline. In this case, the axial velocity

expression, $U_x/U$, at an axial station, x, becomes:

$$\frac{U_x}{U} = \frac{1}{1 - (d_M/d_T)^2} \quad , \tag{3}$$

where $d_M/d_T$ is the local model-to-tunnel diameter ratio at x. The radial velocity expression is more complex. Equation (3) is identical to the results obtained from a one-dimensional conservation of mass approach and reduces to the proper slender body assumption, $U_x/U = 1$, for the free stream case. Figure 2 indicates the extent of the error in the axial velocity at the body surface, by comparing Equation (3) to an exact formulation of $U_x/U$ available using Smith[24] for an ellipsoid-of-revolution. Except for regions near the body nose and tail, the use of Equation (3) for axial velocity does not appear unreasonable. Since the local radial velocity component at the body surface is not required except for predicting those transverse forces produced by means other than the cross flow velocities in the classical slender body approach[21], no attempt has been made to assess the error in local radial velocity between the Goodman and Smith references as was done for the longitudinal velocity in Figure 2. Unfortunately, in attempts to combine the techniques of Goodman and the exact solution of the Neumann problem by Smith, the numerical techniques required quickly become unwieldy. In any case, the tunnel wall interference corrections for ellipsoids-of-revolution predicted by Goodman provide further comparison data.
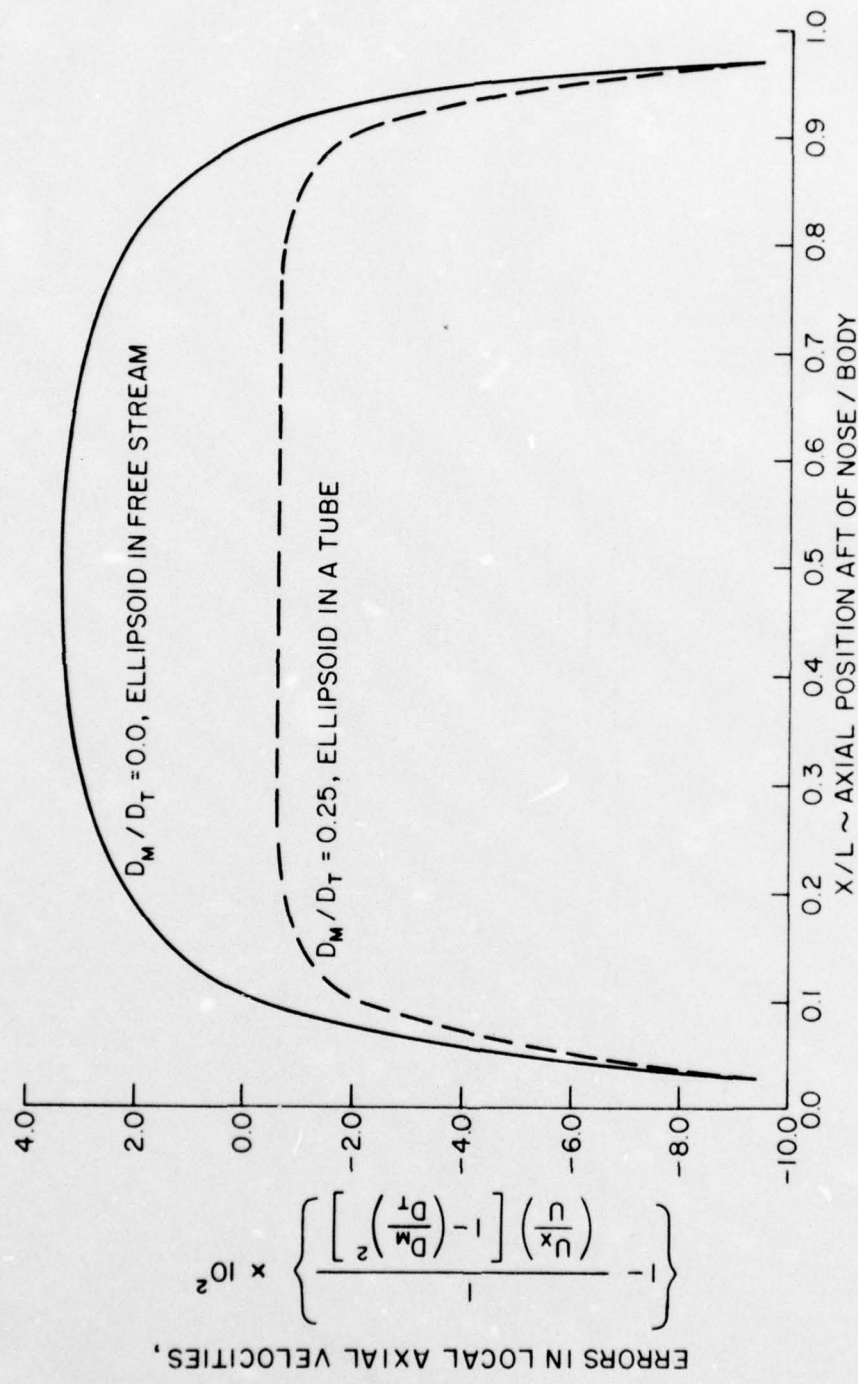
Figure 2  Errors in the Axial Velocity at the Body Surface Using a
One-Dimensional Continuity Equation as Compared to a
Numerical Solution of the Neumann Problem Due to Smith
for an Ellipsoid

Several other approaches are suggested by the literature. Using potential theory, Newman[25] calculates the forces and moments on a slender body moving parallel to an infinite straight wall. In this case, assuming the body-wall separation to be small, and small perturbations about a mean body position, leads to the use of slender body theory for the body-wall combination.

Levine[26] formulates the steady incompressible axisymmetric flow about a body in a tunnel without resorting to the slenderness assumption. However, the body geometry is determined a posteriori, limiting the usefulness of this technique.

## Scope of the Investigation

In order to limit the scope of this investigation, several restrictions and assumptions will be applied. A slender body is assumed. Following Sprieter and Ribner, for simplicity, this assumption restricts the body forces and moments to those predicted by the imposed cross-flow velocities. Only potential flow will be considered. Segel[27] considers the problem of one circular cylinder osciallting laterally inside a second cylinder; the fluid between being considered viscous. The problem is specialized to the case of large Reynolds numbers and the force on the inner cylinder determined. This force consists of a component in-phase with the motion which is of the add-mass type and an out-of-phase component which is the damping force. That part of Segel's add-mass force per unit length which is independent of Reynolds number could be obtained following the inviscid theory suggested by Sprieter and Ribner. However, Segel's damping force per unit length is purely viscous in nature, while that outlined by Sprieter and Ribner is created

by the axial variation of cross-sectional area of the body. Goodman
indicates that the ratio of Segel's viscous damping force to that
predicted by the inviscid theory is of the order:

$$\left(\frac{kf^2}{Re}\right)^{1/2} .$$

(4)

where $k$ equals the reduced frequency, $\frac{\omega \ell}{U}$; Re the Reynolds number
$\frac{U\ell}{\nu}$; and $f$ the body fineness ratio. Typical values of these
quantities for testing with the planar motion mechanism in the ARL
48-inch diameter water tunnel are: $k$ = 1.5, Re = $2.0 \times 10^7$ and,
$f$ = 7.0. Therefore, the viscous damping force per unit length is of
the order of 0.002 the inviscid damping force per unit length and may
safely be ignored.

As a result of these first two assumptions for closed bodies,
which have the property $s(0) = s(\ell) = 0$, the tunnel wall inter-
ference corrections for $C_{L_\alpha}$ and $C_{M_q}$ are lost. However, for bodies
which are not closed, corrections for $C_{L_\alpha}$ and $C_{M_q}$ may be defined.
One approximate method for overcoming this limitation for the closed
bodies forwarded by Sprieter is the definition of an equivalent body
geometry including the body boundary layer thickness. This technique
has been used to successfully predict $C_{L_\alpha}$ for bodies of revolution.
However, the prediction of the boundary layer thickness of an
axisymmetric body in an unrestricted medium or in a tunnel is beyond
the scope of this investigation.

For the present investigation, the body is considered axisymmetric at all axial stations. No wings or other appendiages are considered. Modification of the appropriate cross flow velocity potential to cover a slender wing-body combination in an unrestricted medium has been given by Sprieter, but the cross-flow velocity potential for a slender wing-body combination in a tunnel is unknown.

The present theory is further limited to the prediction of the various stability derivatives, and thus the tunnel wall interference corrections, at the mean body position, where the model and tunnel centerlines coincide.

CHAPTER II


THEORETICAL CONSIDERATIONS


## Introduction to Slender Body Theory

The approximate theory for the flow past a slender body-of-revolution, elongated in the direction of flight, which is generally known as "Slender Body Theory" was introduced by Munk for the calculation of the aerodynamic forces on airships. Jones[28] extended this theory to the study of low-aspect-ratio pointed wings and Ribner applied it to determine the stability derivaties of low-aspect-ratio triangular wings. Sprieter further extended the theory to the study of slender wing-body combinations. Finally, Adams and Sears[29] have reviewed slender body theory, its limitations and extension extensively. In all these studies, the essential point in the study of bodies or wings by "Slender Body Theory" is the fact that, near the body, the flow is approximately two-dimensional when viewed in planes perpendicular to the direction of motion. This follows directly from the nature of the slender body.

Laplace's Equation in cylindrical coordinates for an incompressible flow is well known and may be written:

$$\phi_{xx} + \phi_{rr} + \frac{1}{r}\,\phi_r + \frac{1}{r^2}\,\phi_{\theta\theta} = 0 \quad , \tag{5}$$

where $\phi$ the velocity potential is a function of the independent variables $x$, $r$, and $\theta$ . A coordinate system is presented in

Figure 3. When written in the form of Equation (5), the subscripts x, r, θ indicate partial differentation with respect to that variable. The solution of Equation (5), given the boundary condition of no normal velocity at the body surface, is the Neumann problem. For a general axisymmetric body, the accurate solution of the Neumann problem requires the integral equation formulation and numerical integration techniques of Smith. In avoiding the complexity of Smith's technique "Slender Body Theory" in its classical presentation[1], begins by neglecting the term $\phi_{xx}$ in Equation (5), leaving an approximate equation in the rθ or cross flow plane of Figure 3 of

$$\phi_{rr} + \frac{1}{r} \phi_r + \frac{1}{r^2} \phi_{\theta\theta} = 0 \quad . \tag{6}$$

Equation (6), then, is identically the continuity equation in the cross flow variables r and θ. Justification for this simplification is the slender elongated form of the body. Intuitively, since the cross-sectional area of the body may vary only slowly in the x-direction, it is clear that, $\phi_{xx}$, which is the rate of change of that perturbation velocity $\phi_x$ in the same direction must also be small, at least near the body surface. Near the nose and tail of the body, the accuracy of this assumption is questionable, since the local longitudinal curvature of the body, and hence $\phi_{xx}$, may be rather large. These features are illustrated by Figure 2. Indeed, the inaccuracy of this assumption near the body nose and tail is one reason for predicting tunnel wall interference corrections rather than predicting absolute values for the stability derivatives from slender body theory.
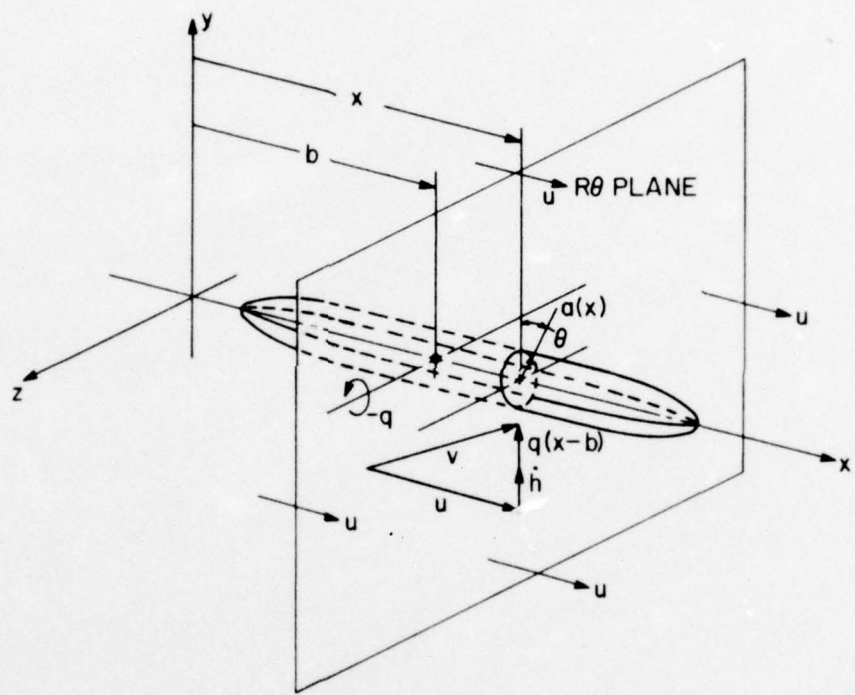
Figure 3   The Problem Coordinate System

The argument for proceeding from Equation (5) to Equation (6) can be made more precisely by considering a non-dimensional form of Equation (5). Let

$$\bar{x} = x/\ell \qquad \bar{r} = r/d \qquad \text{and} \qquad \bar{\phi} = \phi/U\ell , \qquad (7)$$

where the overbar indicates a non-dimensional parameter following Appendix A. Upon substituting Equation (7) into Equation (5), one obtains

$$\left(\frac{d}{\ell}\right)^2 \bar{\phi}_{\bar{x}\bar{x}} + \bar{\phi}_{\bar{r}\bar{r}} + \frac{1}{\bar{r}}\bar{\phi}_{\bar{r}} + \frac{1}{\bar{r}^2}\bar{\phi}_{\theta\theta} = 0 . \qquad (8)$$

It is clear that for sufficiently large values of the fineness ratio, $\ell/d$, the leading term of Equation (8) may be neglected when compared to the remaining terms. In this case, Equation (8) becomes a non-dimensional form of Equation (6).

In any application of slender body theory, the definition of a velocity potential, $\phi$, satisfying Equation (6) and of the appropriate boundary conditions in the $r\theta$ plane at any axial station $x$ are required. From this velocity potential, $\phi$, the pressures on the body periphery at $x$, and hence the local incremental body forces are available. Axial variations in $\phi$ result from a variable body cross-sectional area distribution along the body $x$ axis. In Figure 3, this axial variation of $\phi$ is equivalent to the body moving through a stationary $r\theta$ plane with a velocity U, or conversely moving the $r\theta$

plane past the body at a velocity U. This interpretation has the interesting property of turning a steady three-dimensional problem into an unsteady two-dimensional one. Determination of the total body lift and pitching moment follows from the integration of the local incremental body lift over the body length. Since the local body lift increment follows from Equation (6), no allowance can be made for lift and pitching moment contributions to the total for flows other than the cross flows without resorting to the perturbation techniques of Goodman.

The use of slender body theory to predict the tunnel wall interference corrections reduces the problem to defining the appropriate potential form satisfying Equation (6) subject to boundary conditions reflecting the total body motions.

## Development of the Body Lift and Pitching Moments from Slender Body Theory

In the $r\theta$ plane of Figure 3, the total cross-flow velocity, $\dot{Z}_o$, is governed by the total body motion assumed. Generally, this cross-flow velocity, $\dot{Z}_o$, at $x$ is created by a body plunging motion, $\dot{h}$, perpendicular to the x-axis, and a simultaneous rotation $\theta_1$ at an angular rate $\dot{\theta}_1$ or $q$, about a point $b$ on the body x-axis, as shown. Thus, at any axial station $x$, a first-order approximation of the total cross-flow velocity, $\dot{Z}_o$, in the $r\theta$ plane is

$$\dot{Z}_o(x,t) = \dot{h}(t) + q(t)(x - b) . \tag{9}$$

In Figure 3, $U$ is the constant free stream or unblocked tunnel velocity. A small angle assumption is introduced by restricting the magnitude of $\dot{Z}_o$ in Equation (9) to values much less than $U$. It is convenient

to decompose the local body motion of Equation (9) into a plunging motion where $q = \dot{q} = 0$ and a pitching motion where $h = \ddot{h} = 0$. For the plunging motion Equation (9) reduces to

$$\dot{Z}_o(x,t) = \dot{h}(t) \quad , \quad q(t) = 0. \tag{10}$$

Equation (10) may be related to the body angle-of-attack, $\alpha$, since as a result of the small angle assumption and by definition:

$$V \simeq U = \text{constant}$$

and

$$\dot{Z}_o(x,t) = \dot{h}(t) \simeq U \alpha_o(t) \tag{11}$$

Sinilarly for the pitching motion Equation (9) reduces to

$$\dot{Z}_o(x,t) = q(t) \quad (x = b), \quad \dot{h}(t) = 0 \quad . \tag{12}$$

Again, the small angle assumption, of $\dot{Z}_o(x,t) \ll U$ limits the validity of Equation (12) to small angular displacements about the mean body position. The mean body position being defined as the model and tunnel centerlines coincident.

Another result of the small angle assumption is that in the $r\theta$ plane of Figure 3, the body cross-sections are approximately cylindrical. Looking downstream with x-axis and free stream velocity of Figure 3 into the page at the instant the model and tunnel centerlines coincide, the $r\theta$ plane coordinate system and problem geometry is shown in

Figure 4. It should be noted that the cross sections are only
approximately cylindrical, and the use of a velocity potential based
on that cylindrical cross-section only applies strictly when the model
and tunnel centerlines do coincide. For example, in the unrestricted
medium of Figure 4a, rotation about b as defined by Equation (12)
results in the body cross sections becoming slightly elliptical in the
$r\theta$ plane. For the model in the tunnel, Figure 4b, the body rotation
further complicates the picture; the body cross-section being
eccentric in the tunnel. That is, even if the body cross-section were
cylindrical as in Figure 4b, it would still be displaced from the
tunnel centerline as a function of x and t. In addition, the body
plunging motion as defined by Equation (10) displaces the model and
tunnel centerlines as a function of t alone. Peirce considers a
similar problem in letting the resultant velocity V of Figure 3 be
the free-stream or unblocked tunnel velocity and considering the body
to be a constant angle-of-attack. Since the $r\theta$ plane is now perpen-
dicular to V, the body cross-sections are slightly elliptical and
displaced from the tunnel centerline. By limiting the theory to small
angle of attacks, Peirce also neglects the eccentricity of the body
cross-sections and displacement from the tunnel centerline.

A simple potential form satisfying Equation (6) and the geometry
of Figure 4 is the doublet. Then for the absolute flow about a
cylinder moving through the unrestricted medium of Figure 4a, the
velocity potential is given by

a) MODEL IN FREE STREAM
OR UNRESTRICTED
MEDIUM

b) MODEL IN A
TUNNEL
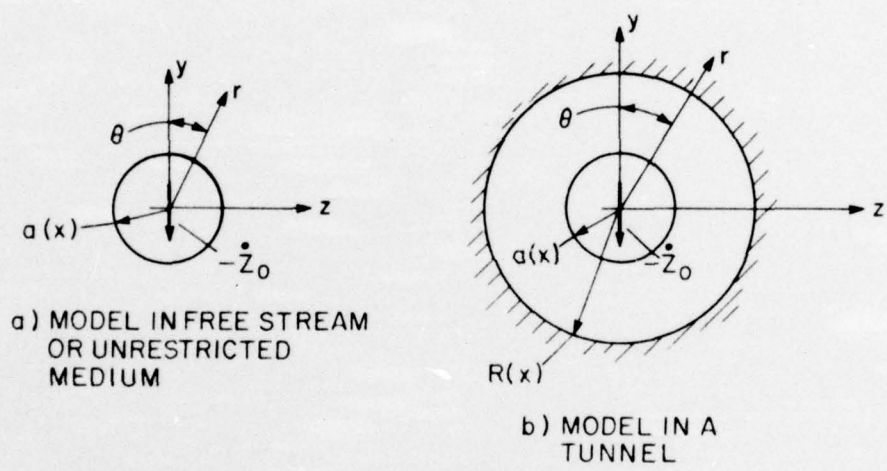
Figure 4   The Problem Coordinate System in the $r\theta$ Plane Looking
Downstream with the  x  Axis into the Page

$$\phi_{FS} = \frac{\mu(x)}{r} \cos \theta \ . \tag{13}$$

Similarly, for the absolute flow about a cylinder moving inside a second cylinder as shown in Figure 4b, one obtains the velocity potential

$$\phi_{IT} = \mu(x) \ \{\frac{1}{r} + \frac{r}{R^2}\} \ \cos \theta \ , \tag{14}$$

where $\mu(x)$ is the doublet strength defined by the appropriate boundary conditions on the body surface and tunnel walls.

In the $r\theta$ plane of Figure 4, there can be no flow through the cylindrical surface element defined by $a(x)$. Mathematically, the boundary condition on the body surface, $a(x)$ is written

$$\phi_r = \frac{\partial \phi}{\partial r} = \dot{Z}_o(x,t) \ \cos \theta \ \text{at} \ r = a(x), \tag{15}$$

where $\phi_r$ equals the radial velocity component and $\dot{Z}_o(x,t)$ is defined by either Equation (10) or Equation (12). In addition, for the cylinder moving in the unrestricted medium, the fluid at infinity must be at rest, or

$$\phi_r = 0 \quad \text{as} \quad r \to \infty \ . \tag{16}$$

For the model in the tunnel, there can be no flow through the tunnel walls defined by $R(x)$. That is,

$$\phi_r = 0 \ \text{at} \ r = R(x), \tag{17}$$

for the body in the tunnel. Performing the indicated operations with Equations (13) and (14) and substituting the appropriate boundary conditions from Equations (15), (16), or (17), one gets for the required velocity potential forms:

$$\phi_{FS} = - \frac{\dot{Z}_o a^2(x)}{r} \cos \theta , \qquad (18)$$

for the body in free stream, and

$$\phi_{IT} = - \frac{\dot{Z}_o a^2(x)}{1-(a/R)^2} \cdot \left\{ \frac{1}{r} + \frac{r}{R^2} \right\} \cos \theta, \qquad (19)$$

for the model in the tunnel, respectively.

Once the velocity potentials are know, the incremental body lift in the $r\theta$ plane, $\frac{dL}{dx}$, can be obtained by integrating the pressure around the body periphery $r = a(x)$. Then,

$$\frac{dL}{dx} = \int_0^{2\pi} \Delta P_a \, a \cos \theta \, d\theta , \qquad (20)$$

where $\Delta P_a$ is the local pressure on the body surface as a function of aximuth angle, $\theta$. Appendix B develops a general Bernoulli Equation relating pressure and fluid velocities in a coordinate system moving with the body permitting use of the velocity potentials of Equations (18) and (19). From this general Bernoulli Equation, Equation (B-7), the incremental pressure at a point in the $r\theta$ plane is

$$\frac{\Delta P}{\rho} = -\frac{\partial \phi}{\partial t} - \frac{1}{2}(\phi_r^2 + \frac{1}{r}\phi_\theta^2) + \dot{Z}_o(\phi_r \cos\theta - \frac{1}{r}\phi_\theta \sin\theta). \quad \text{(B-7)}$$

Performing the indicated operations of Equations (B-7) and evaluating at the body periphery, $r = a$, the local pressure on the body periphery as a function of aximuth angle, $\theta$, becomes

$$\Delta P_a = -\rho \frac{\partial \phi_{FS}}{\partial t} + \frac{1}{2}\{\dot{Z}_o^2 \; 1 - 4\sin^2\theta \; \}, \quad \text{at } r = a \quad \text{(21)}$$

for the model in the unrestricted medium and

$$\Delta P_a = -\rho \frac{\partial \phi_{IT}}{\partial t} + \frac{1}{2}\rho \dot{Z}_o^2 \; \{1 - \frac{4}{1 - (a/R)^2}\sin^2\theta\} \; , \quad \text{at } r = a \quad \text{(22)}$$

for the model in the tunnel.

In Equations (21) and (22), the bracketed term of the right-hand side is the steady state pressure distribution at the body periphery shown in Figure 5a. Upon integration of these bracketed terms as indicated by Equation (20), the resultant pressure disappears, since no pressure forces can occur in potential flow. Indeed, this is a shortcoming of the inviscid slender body theory. Allen and Perkins[30] attempt to ameliorate this difficulty by considering viscous flow in the $r\theta$ plane. The approximate method consists of the addition of a cross-flow drag term to the potential flow incremental body lift. This is based on the assumption that each circular element along the body will experience an additional cross force equal to the drag force of a section operating at a velocity $\dot{Z}_o$. In practice, this approximate
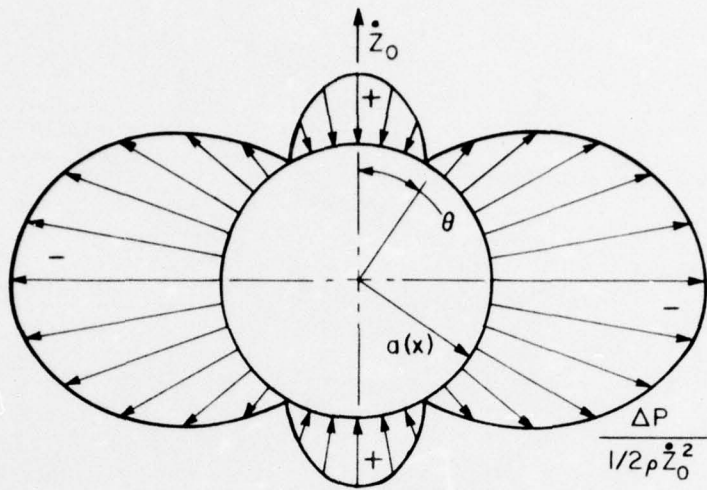
a) STEADY STATE PRESSURE DISTRIBUTION OVER
THE SURFACE OF A CYLINDER
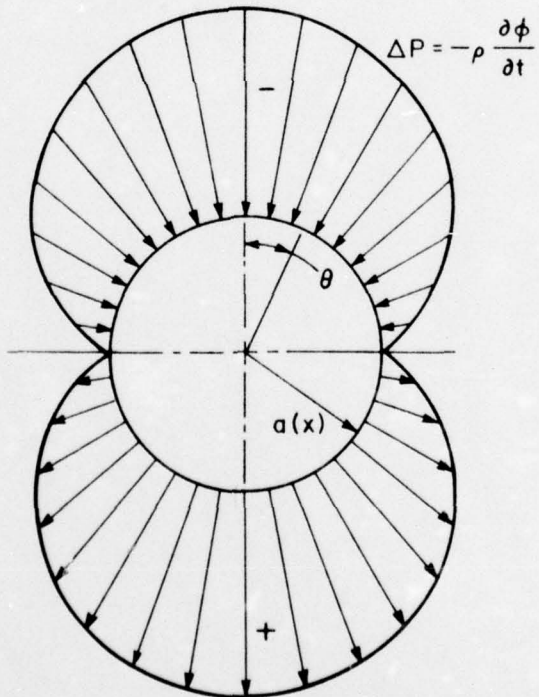
b) ACCELERATION PRESSURE DISTRIBUTION OVER
THE SURFACE OF A CYLINDER

Figure 5   The Pressure Distribution Over the Surface of a Cylinder
in Two-Dimensional Potential Flow

method does give good agreement between measured and calculated lifts. However, when considering potential flows, it is necessary to consider only the acceleration pressures of the form

$$\Delta P_a = -\rho \frac{\partial \phi}{\partial t} \tag{23}$$

shown in Figure 5b. Thus $\Delta P_a$, and hence, the incremental body lift $\frac{dL}{dx}$ can only be generated by changes in body and/or tunnel cross-sections and accelerations in the $r\theta$ plane. By chain rule differentiation the local acceleration in the $r\theta$ plane is

$$\frac{\partial \phi}{\partial t} = U_x \left( a' \frac{\partial \phi}{\partial a} + R' \frac{\partial \phi}{\partial R} \right) + \dot{Z}_o \frac{\partial \phi}{\partial Z_o} , \tag{24}$$

where $U_x$ is the local axial velocity, $a'$ the local body slope and $R'$ the local tunnel wall slope, are all functions of $x$, and where $\ddot{Z}_o = \frac{\partial \dot{Z}_o}{\partial t}$. For a model in a tunnel, the application of Equation (24) to Equation (19), the evaluation at the body periphery, and the integration according to Equation (20) yields the incremental body lift.

$$\left( \frac{dL}{dx} \right)_{IT} = \rho U_x \dot{Z}_o \frac{1 + (a/R)^2}{\left[ 1 - (a/R)^2 \right]^2} S' - 4a \frac{(a/R)^3}{\left[ 1 - (a/R)^2 \right]^2} R'$$

$$\tag{25}$$

$$+ \rho \ddot{Z}_o \left[ \frac{1 + (a/R)^2}{1 - (a/R)^2} \right] S ,$$

where $S = \pi a^2$ is the local body cross-section in the $r\theta$ plane, and $S'$ the local change of that cross section. Both of these quantities are functions of $x$.

The unrestricted medium incremental body length can be obtained from the in-tunnel expression, Equation (25) by letting the tunnel radius approach infinity. Then,

$$\left(\frac{dL}{dx}\right)_{FS} = \lim_{R \to \infty} \left(\frac{dL}{dx}\right)_{IT} = \rho U_x \dot{Z}_o S' + \rho \ddot{Z}_o S . \tag{26}$$

Alternatively, $\left(\frac{dL}{dx}\right)_{FS}$ may be obtained by direct application of Equation (24) to Equation (18), evaluation at the body periphery, and integration according to Equation (20) as was done for the model in the tunnel.

Inclusion of a term proportional to $R'$, the local tunnel radius slope, in Equation (25) for completeness permits estimation of the interference on a body in an axially varying tunnel section such as a nozzle or diffuser. In practice, since most closed-jet tunnels have constant radius test sections, this term is zero for an inviscid fluid solution. However, the term does indicate one approximate method for correcting the lift and pitching moment for the static pressure gradient for the test section.

The static pressure gradient along the tunnel test section is typically of the form presented in Figure 6. Using Bernoulli's Equation and the one-dimensional continuity equation for the unblocked
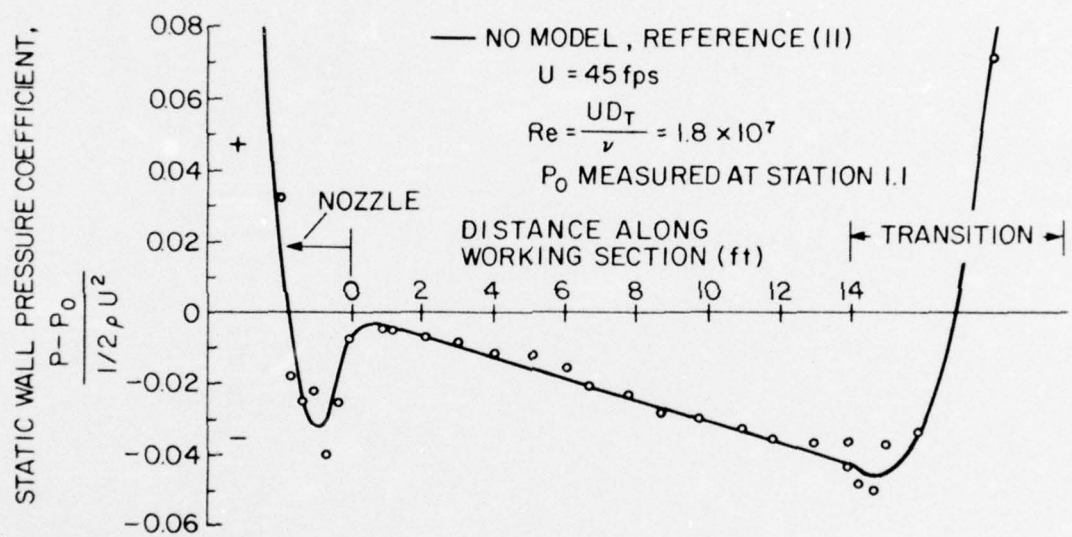
Figure 6   Wall Pressures in the Working Section of the ARL 48.0-inch-
Diameter Water Tunnel

tunnel, this negative static pressure gradient can be considered as an effective decrease in the cross-sectional area due to the growth of the boundary laryer on the test section walls. Then, an equivalent body radius R may be defined:

$$\frac{R}{R_o} = \frac{1}{(1 - C_p)^{1/2}} \quad , \tag{27}$$

where $R_o$ is the tunnel radius at the point the reference static pressure was measured, usually the nozzle throat. R' follows directly from Equation (27)

$$\frac{d}{dx} \left[ \frac{R}{R_o} \right] = \frac{C_p'}{(1 - C_p)^{5/4}} \quad , \tag{28}$$

where $C_p'$ is the local static pressure gradient along the tunnel working section. For the ARL 48-inch diameter water tunnel, $C_p'$ equals −0.003 per foot. Using this $C_p'$ as typical, and a 7:1 fineness ratio ellipsoid of model-to-tunnel diameter ratio 0.25 for the calculations, the contribution of the R' term in Equation (25) to the total is negligible. Thus, even for a real tunnel Equation (25) may be further simplified to

$$\left( \frac{dL}{dx} \right)_{IT} = \rho U_x \dot{Z}_o \frac{1 + (a/R)^2}{\left[ 1 - (a/R)^2 \right]^2} S' + \rho \ddot{Z}_o \left\{ \frac{1 + (a/R)^2}{1 - (a/R)^2} \right\} S, \tag{29}$$

without a loss in accuracy.

From the free-body diagram, Figure 7, the total body lift, L, may be obtained by integrating the appropriate incremental body lifts over the body length $\ell$. That is,

$$L = \int_{x=0}^{x=\ell} \frac{dL}{dx} \, dx \; , \tag{30}$$

where $\frac{dL}{dx}$ is specified by either Equation (26) for the model in the unrestricted medium, or by Equation (29) for the model in the tunnel. Also, the pitching moment, M, about the rotation center, b, may be written

$$M = - \int_{x=0}^{x=\ell} (x - b) \frac{dL}{dx} \, dx \; . \tag{31}$$

## The Stability Derivatives

For a body underoing a plunging motion, the substitution of Equation (26) along with Equation (11) in Equations (30) and (31) yields the total lifts and pitching moments for the body in an unrestricted medium. Then, by non-dimensionalizing following Appendix A, but dropping the overbars for notational simplicity, and expanding the resultant lift and pitching moment coefficients in a linear Taylor series, the stability derivatives for plunging motion in an unrestricted medium are

$$C_{L_\alpha} = 2 \frac{\ell^2}{S_M} \int_{x=0}^{x=1} \left( \frac{U_x}{U} \right)_{FS} \, dS \; , \tag{32}$$
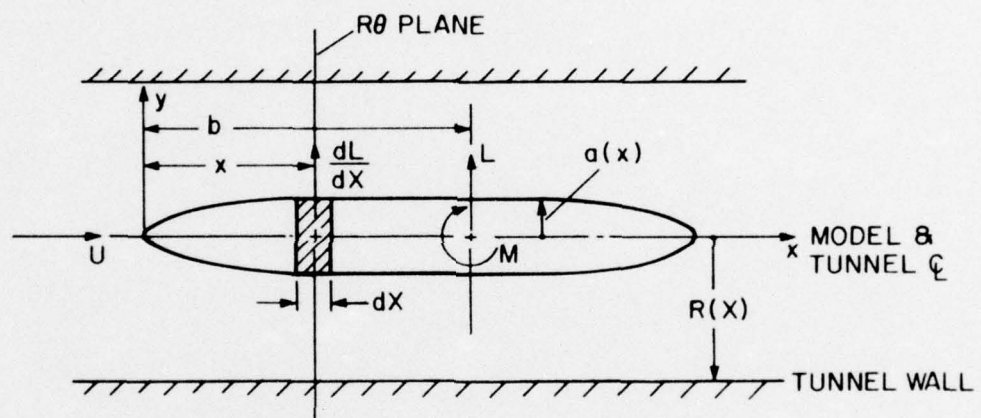
Figure 7    The Coordinate System Perpendicular to the $r\theta$ Plane When
the Model and Tunnel Centerlines Coincide

$$C_{M_{\alpha_{FS}}} = -2 \frac{\ell^2}{S_M} \int_{x = 0}^{x = 1} \left(\frac{U_x}{U}\right)_{FS} (x-b) \, dS \quad , \qquad (33)$$

$$C_{L_{\alpha_{FS}}} = 2 \frac{\ell^2}{S_M} \int_{x = 0}^{x = 1} dV \quad , \qquad (34)$$

and

$$C_{M_{\dot{\alpha}_{FS}}} = -2 \frac{\ell^2}{S_M} \int_{x = 0}^{x = 1} (x-b) \, dV \quad , \qquad (35)$$

where $dV$ is the volume increment, $S\,dx$.

Note that in contrast to slender wing theory which is applied only to wings of increasing span, Equations (32) and (33) may be applied to bodies of revolution in regions of either increasing or decreasing radius, since the Kutta condition does not apply to bodies-of-revolution. Thus, in general, the lift and pitching moment for a body-of-revolution is different from that of a wing of equal planform.

Repeating the above procedure using Equation (29), provides one with stability derivatives from the plunging motion for the model in the tunnel. Thus,

$$C_{L_{\alpha_{IT}}} = 2 \frac{\ell^2}{S_M} \int_{x = 0}^{x = 1} \frac{1 + (a/R)^2}{\left[1 - (a/R)^2\right]^2} \left[\frac{U_x}{U}\right]_{IT} dS \quad , \qquad (36)$$

$$C_{M_{\alpha_{IT}}} = -2 \frac{\ell^2}{S_M} \int_{x=0}^{x=1} \frac{1 + (a/R)^2}{\left[1 - (a/R)^2\right]^2} \cdot \left(\frac{U_x}{U}\right)_{IT} (x-b)dS, \quad (37)$$

$$C_{L_{\dot{\alpha}_{IT}}} = 2 \frac{\ell^2}{S_M} \int_{x=0}^{x=1} \frac{1 + (a/R)^2}{1 - (a/R)^2} \, dV, \quad (38)$$

and

$$C_{M_{\dot{\alpha}_{IT}}} = -2 \frac{\ell^2}{S_M} \int_{x=0}^{x=1} \frac{1 + (a/R)^2}{1 - (a/R)^2} (x-b) \, dV \quad . \quad (39)$$

The free stream stability derivatives may also be obtained by letting the tunnel radius, R, approach infinity in Equations (26) to (39).

For pure pitching motion, the substitution of Equation (26) along with Equation (12) in Equations (30) and (31) provides the appropriate lifts and pitching moments. Then, following the non-dimensionalization and expansion procedures outlined above, the stability derivatives in the unrestricted medium from the pitching motion become

$$C_{L_{q_{FS}}} = 2 \frac{\ell^2}{S_M} \int_{x=0}^{x=1} \left(\frac{U_x}{U}\right)_{FS} (x-b) \, dS \quad , \quad (40)$$

$$C_{M_{q_{FS}}} = -2 \frac{\ell^2}{S_M} \int_{x=0}^{x=1} \left(\frac{U_x}{U}\right)_{FS} (x-b)^2 \, dS \quad , \tag{41}$$

$$C_{L_{\dot{q}_{FS}}} = 2 \frac{\ell^2}{S_M} \int_{x=0}^{x=1} (x-b) \, dV \quad , \tag{42}$$

and

$$C_{M_{\dot{q}_{FS}}} = -2 \frac{\ell^2}{S_M} \int_{x=0}^{x=1} (x-b)^2 \, dV \quad . \tag{43}$$

In the tunnel, the stability derivatives from Equation (29) for the pitching motion of the body are

$$C_{L_q} = 2 \frac{\ell^2}{S_M} \int_{x=0}^{x=1} \frac{1 + (a/R)^2}{\left[1 - (a/R)^2\right]^2} \left(\frac{U_x}{U}\right)_{IT} (x-b) \, dS \quad , \tag{44}$$

$$C_{M_q} = -2 \frac{\ell^2}{S_M} \int_{x=0}^{x=1} \frac{1 + (a/R)^2}{\left[1 - (a/R)^2\right]^2} \cdot \left(\frac{U_x}{U}\right)_{IT} (x-b)^2 \, dS \quad , \tag{45}$$

$$C_{L_{\dot{q}}} = 2 \frac{\ell^2}{S_M} \int_{x=0}^{x=1} \frac{1 + (a/R)^2}{1 - (a/R)^2} (x-b) \, dV, \tag{46}$$

and

$$C_{M_{\dot{q}}} = -2 \frac{\ell^2}{S_M} \int_{x=0}^{x=1} \frac{1 + (a/R)^2}{1 - (a/R)^2} (x-b)^2 \, dV \quad . \tag{47}$$

However, because of the inaccuracies inherent in the slender body assumptions, it is reasonable to predict tunnel interference corrections rather than to attempt to predict absolute values of the stability derivatives from Equations (32) to (47). It is expected that experimentally-determined derivatives would prove to be more accurate.

For example, $C_{L_\alpha}$ is known to be seriously in error when compared with experimentally determined values of $C_{L_\alpha}$ for closed bodies-of-revolution. To ameliorate this difficulty, numerous techniques have been suggested including:

(1) The inclusion of the cross-flow drag coefficient in the definition of the incremental body lift, by Allen and Perkins,

(2) The inclusion of the body boundary thickness in the definition of the body geometry by Sprieter, and

(3) The resorting to strictly empirical prediction techniques by Abkowitz[31].

These techniques have met with varying degrees of success.

Similarly, for $C_{M_\alpha}$, the development following Sprieter differs from the more exact formulation of Munk by a factor $(K_2 - K_1)$ where $K_2$ and $K_1$ are the so-called transverse and longitudinal "add mass" coefficients, respectively. In addition, Munk's formulation for $C_{M_\alpha}$ is known to over-estimate $C_{M_\alpha}$ by about 13 percent due to real fluid effects.

CHAPTER III


THE TUNNEL WALL INTERFERENCE CORRECTIONS


By definition, the tunnel wall interference correction factors
are the ratio of the stability derivatives for the model in the tunnel
to those for the model in an unrestricted medium. Then, for the
plunging motion Equation (11), these corrections become

$$\frac{C_{L_{\alpha_{IT}}}}{C_{L_{\alpha_{FS}}}} = \frac{\text{Equation (36)}}{\text{Equation (32)}} \qquad ,$$

$$\frac{C_{M_{\alpha_{IT}}}}{C_{M_{\alpha_{FS}}}} = \frac{\text{Equation (37)}}{\text{Equation (33)}} \qquad ,$$

(48)

$$\frac{C_{L_{\dot{\alpha}_{IT}}}}{C_{L_{\dot{\alpha}_{FS}}}} = \frac{\text{Equation (38)}}{\text{Equation (34)}} \qquad ,$$

and

$$\frac{C_{M_{\dot{\alpha}_{IT}}}}{C_{M_{\dot{\alpha}_{FS}}}} = \frac{\text{Equation (39)}}{\text{Equation (35)}} \qquad .$$

Similarly for the pitching motion, Equation (12), the following corrections apply:

$$\frac{C_{L_{q_{IT}}}}{C_{L_{q_{FS}}}} = \frac{\text{Equation (44)}}{\text{Equation (40)}} \quad ,$$

$$\frac{C_{M_{q_{IT}}}}{C_{M_{q_{FS}}}} = \frac{\text{Equation (45)}}{\text{Equation (41)}} \quad ,$$

$$\frac{C_{L_{\dot{q}_{IT}}}}{C_{L_{\dot{q}_{FS}}}} = \frac{\text{Equation (46)}}{\text{Equation (42)}} \quad ,$$

(49)

and

$$\frac{C_{M_{\dot{q}_{IT}}}}{C_{M_{\dot{q}_{FS}}}} = \frac{\text{Equation (47)}}{\text{Equation (43)}} \quad .$$

CHAPTER IV


APPLICATION OF THE DEVELOPED THEORY


The definition of the general axisymmetric body implies that the body radius as a function of the axial station  x  along the body cannot easily be defined by a simple mathematical function, but rather must be specified numerically.  Generally, models for which stability derivatives are desired will fall into this category.  In addition, it is possible to define three separate axial velocity distributions at the body surface,  $U_x/U$, for use in the $C_{L_\alpha}$  and  $C_{M_\alpha}$  equations. First, one may assume  $U_x/U$ = 1.  This assumption corresponds to that of classical slender body theory where the longitudinal velocity everywhere on the body surface is equal to the free stream velocity.  This implies small body thicknesses and curvatures compared to overall body length. Alternatively, one may choose to use Equation (3)


$$\frac{U_x}{U} = \frac{1}{1 - (d_M/d_T)^2} \quad , \tag{3}$$


for the model in the tunnel.  Figure 2 shows that this is a somewhat better assumption for the axial velocity distribution for a body in a tunnel than  $U_x/U$ = 1.  Finally, one may consider  $U_x/U$ defined from the numerical solution of the Neumann problem by Smith.

The effect of these three different axial velocity functions on the $C_{M_\alpha}$ integrand for an ellipsoid may be seen in Figure 8. While an exact evaluation of the integrals may be available for simple body shapes and the slender body theory axial velocity assumption, $U_x/U = 1$, the integrations in Equations (32) to (47) involving more complex body shapes and axial velocity assumptions would be tedious and time-consuming, at best. The modern high-speed digital computer offers a more rewarding approach encompassing all the possible axial velocity assumptions and body shapes, by means of numerical integration.

The body shape and the axial velocity $U_x/U$; and hence, the integrands of Equations (32) to (47) may be specified as a function of $x$ using the mathematical equivalent of the draftman's spline curve. This mathematical spline curve[32] accurately defines the curve and its first and second derivatives, from a set of points. The only constraint on the use of the mathematical spline curve being the points to be fitted must be single-valued in the independent variable.

Also, numerous integration techniques, e.g., Runge-Kutta, Simpson's Rule, Gauss-Legendre, etc., are available. The technique chosen for the calculations of this thesis, primarily for its speed and accuracy, was the Gauss-Legendre Quadrature[33].

Then, the procedure used for the evaluation of the integrals, Equations (32) to (47) regardless of the body shape or axial velocity assumption used was as follows:
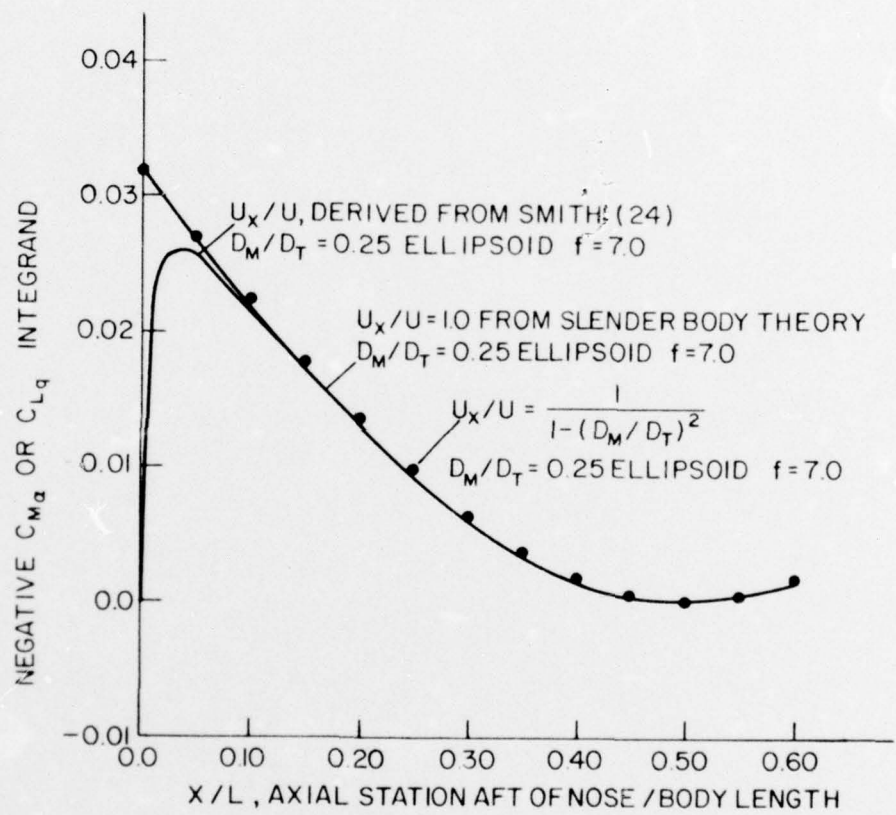
Figure 8  Pitching Moment Coefficient Integrands as a Function of
Body Axial Coordinate  x

(1) The body shape and axial velocity as a function of  x
were specified numerically and fitted using the mathematical
spline curve techniques.

(2) From this spline-fitted data, the integrands required in
Equations (32) to (47) were defined as a function of  x
and similarly fitted using the mathematical spline curve
techniques.

(3) Evaluation of the integrals was accomplished using the
Gauss-Legendre Quadrature.

The accuracy of this procedure was checked by computing the volume of
an ellipsoid and comparing it with known exact values for the ellipsoid
volume.  This comparison produced errors of less than 0.03 percent.
In addition, since tunnel interference corrections were to be defined
for ellipsoids for comparison with experimental results later, and
for which the required integrands could be defined exactly as a
function of  x,  a comparison was made with the integrands obtained
following the above procedure.  There were no observable differences,
and the technique may be safely applied to any axisymmetric
body-of-revolution.

The majority of the theoretical work was specialized to the
ellipsoids-of-revolution for two reasons.  First, the integrands of
Equations (32) to (41) could be formulated exactly from the
equation describing the ellipsoid.

$$S = 4S_M x (1-x), \quad 0 \leq x \leq 1 , \qquad (50)$$

where  x,  the axial coordinate, is measured from the nose.  In this case, a step-by-step evaluation of the numerical techniques outlined is possible.  Secondly, a significant, though limited, body of data[1],[2] both theoretical and experimental are available for comparison with the present simple theory.  Such data are not available for any other body shape.

The listed assumption, presented in the scope of the investigation, and the choice of the ellipsoidal body shape imply several things. Since the ellipsoid is a closed body, $C_{L_\alpha}$ is lost.  Similarly, in the choise of the body midpoint as the rotation center, fore and aft body symmetry produces the loss of corrections for $C_{M_q}$, $C_{L_{\dot{q}}}$, and $C_{M_{\dot{\alpha}}}$ .  In the case of a body with no fore and aft symmetry, tunnel interference corrections for these derivatives could be defined.  Of course, the selection of a different rotation center for the ellipsoids would permit the definition of tunnel interference corrections for $C_{M_q}$, $C_{M_{\dot{\alpha}}}$ and $C_{L_{\dot{q}}}$ but care must be exercised in interpreting the resultant corrections. Also, from comparison of Equation (37) and (40),      $C_{L_q} = - C_{M_\alpha}$; thus, for these stability derivatives the tunnel interference corrections are identical.

The theoretical tunnel wall interference corrections developed for the ellipsoids-of-revolution from the present theory are presented in Figures 9 and 10 as a function of the maximum model to tunnel diameter ratio.  For the corrections involving the axial velocity at the body surface, $C_{M_\alpha}$ and $C_{L_q}$, Figure 9 shows the effect of each of the three possible axial velocity assumptions on the correction.
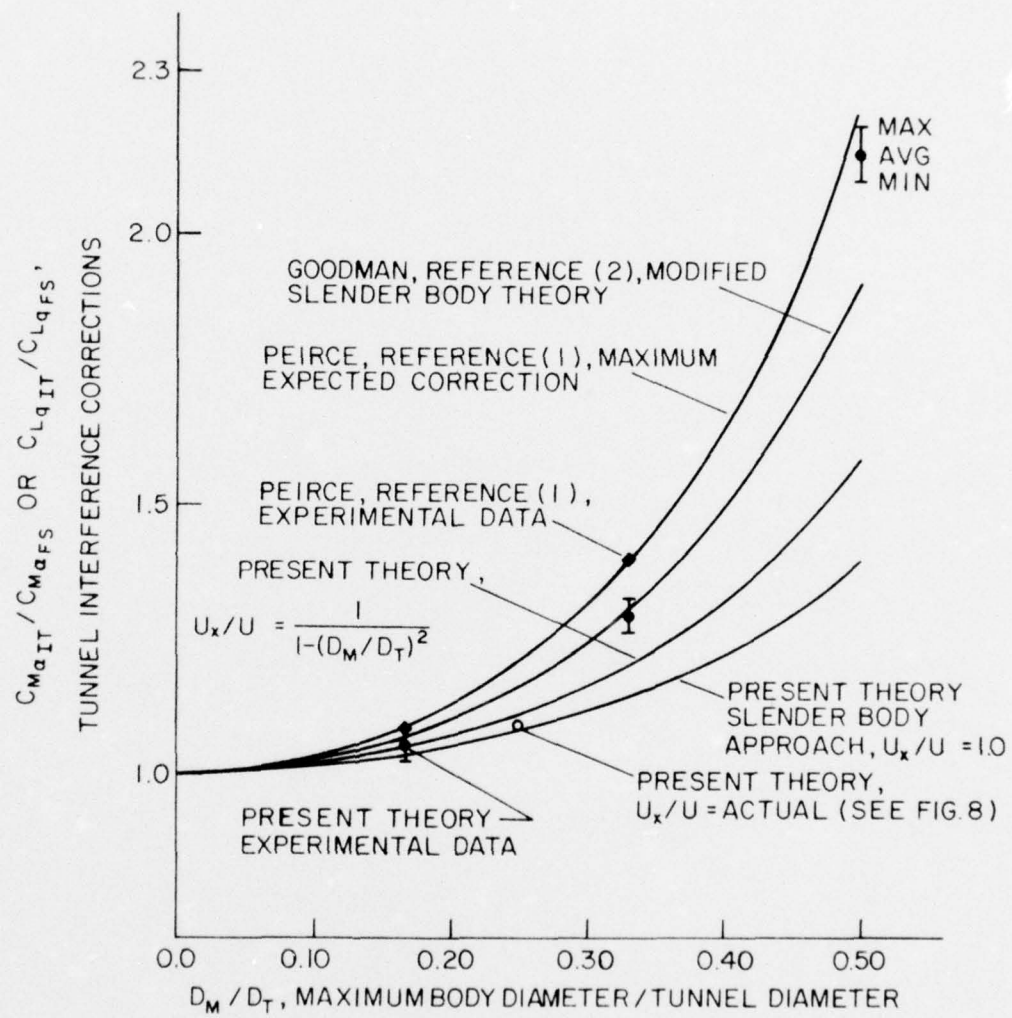
Figure 9   Tunnel Wall Interference Corrections for the Static
Pitching Moment Coefficient Per Degree as a Function of
the Model-to-Tunnel Diameter Ratio
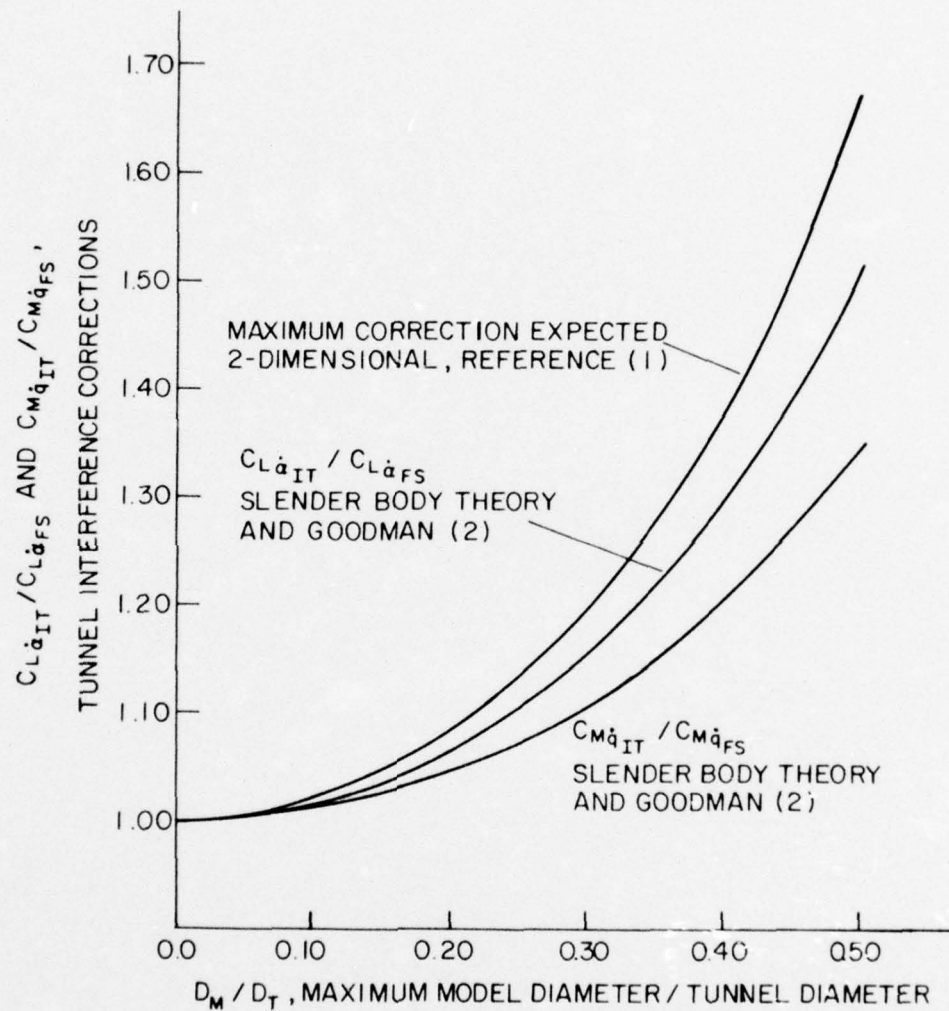
Figure 10  Tunnel Wall Interference Corrections for the Acceleration Stability Derivative as a Function of the Model-to-Tunnel Diameter Ratio

Also, Figure 9 includes the corrections from Goodman for an ellipsoid and the maximum tunnel interference correction for $C_{M_\alpha}$ of Peirce, Equation (2).

Similarly, Figure 10 presents the theoretical corrections for the acceleration stability derivatives, $C_{L_{\dot\alpha}}$ and $C_{M_{\dot q}}$. Note that in Figure 10, the corrections from Goodman and the present theory are identical. Also, Figure 10 includes a maximum tunnel wall interference correction for $C_{L_{\dot\alpha}}$ or $C_{M_{\dot q}}$. Following Peirce and assuming the maximum correction factor occurs at the maximum local model/tunnel diameter ratio, the maximum $C_{L_{\dot\alpha}}$ or $C_{M_{\dot q}}$ interference correction is defined as

$$\frac{1 + (d_M/d_T)^2_{max}}{1 - (d_M/d_T)^2_{max}} \tag{51}$$

This correction, corresponds to an infinite cylinder oscillating inside a second cylinder.

These maximum corrections, Equation (2) for $C_{L_\alpha}$, $C_{M_\alpha}$, $C_{L_q}$, and $C_{M_q}$ and Equation (51) for $C_{L_{\dot\alpha}}$, $C_{M_{\dot\alpha}}$, $C_{L_{\dot q}}$, and $C_{M_{\dot q}}$ may be considered as applicable to a body with a prismatic coefficient, $\alpha$, of 1.0. The ellipsoid which was used to evaluate the various theories have a prismatic coefficient of 0.667. This prismatic coefficient, 0.667, is close to the minimum for typical hydrodynamic bodies-of-revolution. It may be that the present theory and that of Goodman represent minimum tunnel wall interference corrections.

However, some care must be exercised in making this statement, since the prismatic coefficient does not specify the distribution of cross-sectional area, S, along the body x-axis. Indeed, the ellipsoidal distribution, Equation (50), is but one of many possible distributions with a prismatic coefficient of 0.667. Goodman indicates that correction calculations made for a circular cylinder with ogival ends produces only minor deviations from the tunnel interference correction for the ellipsoids, but no further specification of this body is given. In any case, for the purposes of this thesis, no attempt has been made to assess the effect of cross-sectional area distribution at a constant prismatic coefficient on the tunnel interference corrections.

CHAPTER V


EXPERIMENTAL STUDIES


The Experimental Apparatus

In order to provide a comprehensive evaluation of the developed
slender body theory, at least three geometrically similar models of
varying model-to-tunnel diameter ratios would have to be fabricated for
testing with the ARL Planar Motion Mechanism in the 48.0-inch-diameter
water tunnel. Since model fabrication for tests with the Planar Motion
Mechanism and the testing itself are quite expensive and time consuming,
it was decided that at least a partial confirmation could be obtained
from wind tunnel tests. Although no evaluation of the dynamic stability
derivatives, $C_{L_{\dot{\alpha}}}$ , $C_{M_{\dot{\alpha}}}$ , $C_{L_{\dot{q}}}$ , and $C_{M_{\dot{q}}}$ could be obtained, tests
yielding model pitching moments as a function of angle of attack for
three ellipsoids-of-revolution would provide experimental tunnel
interference corrections for comparison with the various theories
of Figure 9.

All the experimental work was performed in the subsonic wind
tunnel operated by the Department of Aerospace Engineering, The
Pennsylvania State University.

This tunnel is a closed-return type tunnel which may be operated
in either a closed-throat or an open-jet test section configuration.
In the closed-throat mode, the rectangular test section measures 4 ft.
high, 5 ft. wide and 6 ft. long. Maximum closed-throat test section

velocities of the order of 180 ft./sec. may be obtained, but safe
practical speeds are somewhat lower. Associated with this tunnel is
a permanent six-component pyramidal balance system manufactured by
Aerolab., Incorporated, of Gaithersburg, Maryland. Unfortunately, for
the present experiments, the very low moments of less than 2 ft. lbs.
maximum generated by the ellipsoids precluded the use of this balance
except for the largest of the ellipsoids. Since it was desirable to
make all moment measurements with a common measurement system, the
permanent wind tunnel balance was not used except as a device for
setting the body angles of attack.

The experimental phase of this thesis was divided into two major
sections. First, the ellipsoid pitching moment coefficients as a
function of angle-of attack were obtained in an essentially unrestricted
medium; i.e., the model's maximum cross-section was sufficiently small
when compared to that of the tunnel to justify neglecting any residual
tunnel interference. Secondly, similar pitching moment data were
obtained for the ellipsoids in a 12.0-inch diameter tube inserted in the
tunnel as shown in Figure 11, where the tunnel interference was
predicted to be significant. From these tests, the ratio of the
pitching moment coefficient slope for the ellipsoids in the tube and
unrestricted medium was the experimental tunnel wall interference
correction for comparison with the theories of Figure 9.

To model a tunnel test section, the 12.0-inch diameter tube 5.0
ft. long was rolled from 0.0625 in. thick aluminum sheet. Stiffening
rings were provided for fastening the tube in the tunnel test section
as shown in Figure 11. In addition, a crude inlet fairing was installed
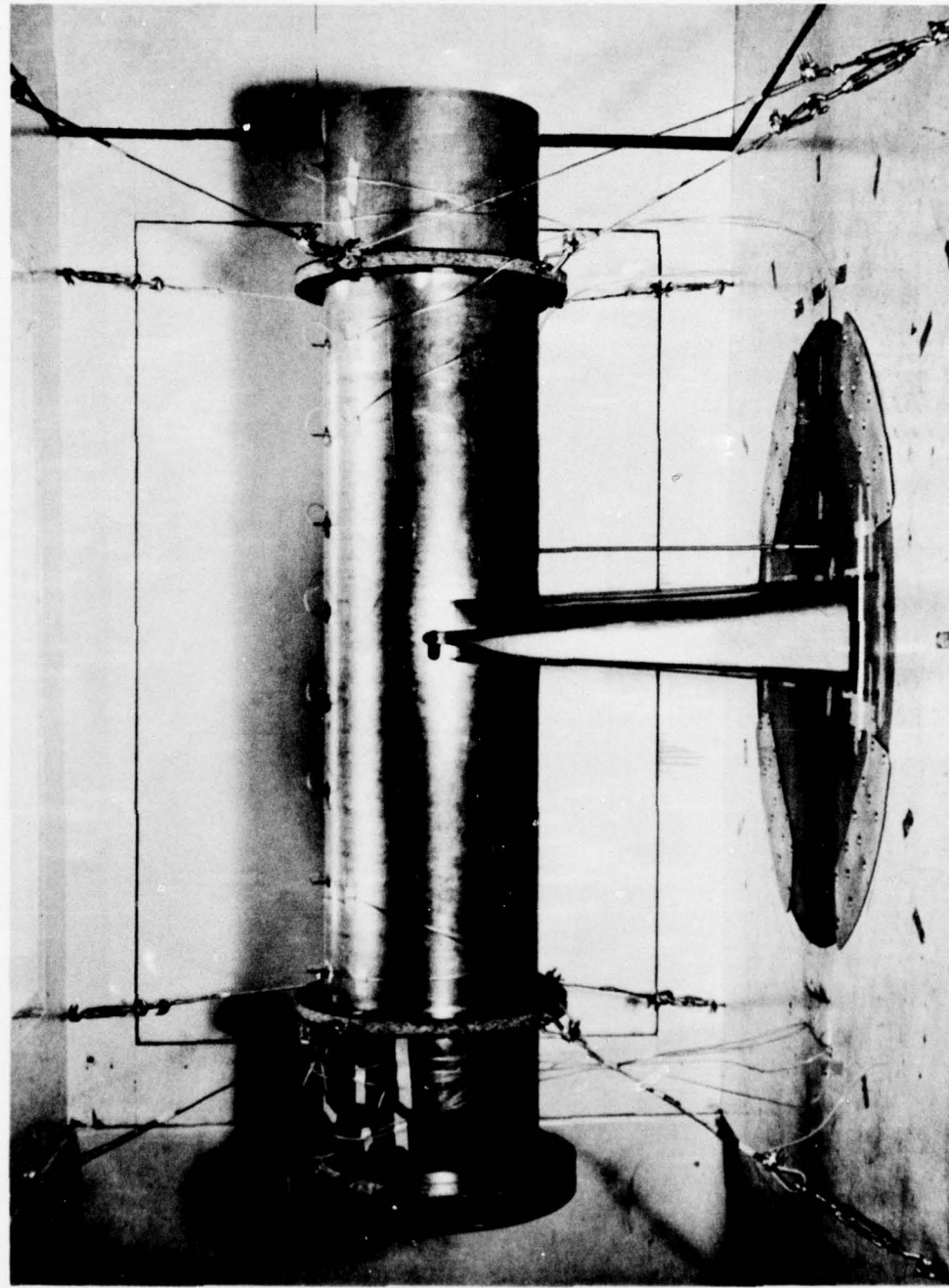
Figure 11  The Rolled-Aluminum Tube Simulating a Tunnel Test Section

in an attempt to prevent any local flow separation occurring as a result of tube misalignment in the tunnel. To insure that the tube was a fair representation of a tunnel test section, the velocity profile near the tube inlet, Figure 12, and the wall static pressure gradient along the tube, Figure 13, were obtained. From comparison of these figures with similar data for typical tunnels, it was clear that the tube was representative of typical test sections.

As models, three ellipsoids-of-revolution of fineness ratio 7, Figure 14, and with maximum diameters of 2.0, 4.0 and 6.0 inches, resulting in model to tunnel diameter ratios of 0.1667, 0.3333 and 0.500, respectively, were fabricated from white pine. Boundary layer trip wires were installed on all the models at approximately $0.05\ell$. The boundary layer trip wires were considered necessary for two reasons. First, in order to insure the same flow conditions over the models, it was desirable to conduct at least some of the tests at a Reynolds number common to all the models. Since the largest practical common geometric Reynolds number as defined by practical tunnel speeds and the 2.0 in. diameter model was approximately $10^6$, it was possible that consideration of an effective Reynolds number could result in models being tested in the critical Reynolds number range for transition from laminar to turbulent flow over the body. No tunnel turbulence factor measurements were available for defining an effective Reynolds number of the tunnel used. However, subsequent pitching moment tests of the 6.0-inch diameter ellipsoid with and without the trip indicated no measurable differences
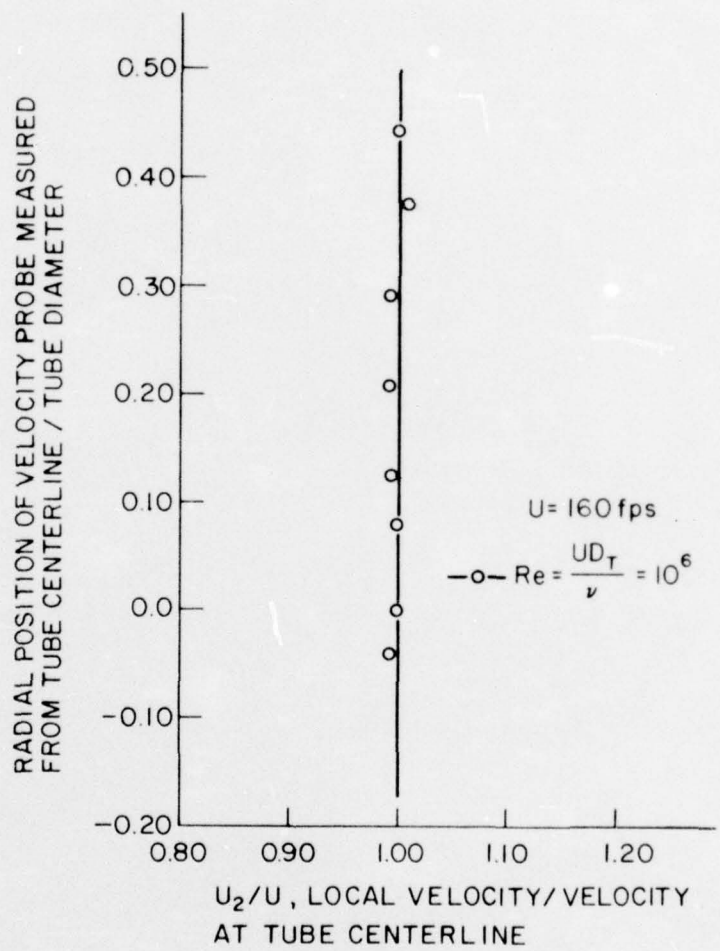
Figure 12   Tube Velocity Profile at 3.0 in. Aft of the Tube Inlet
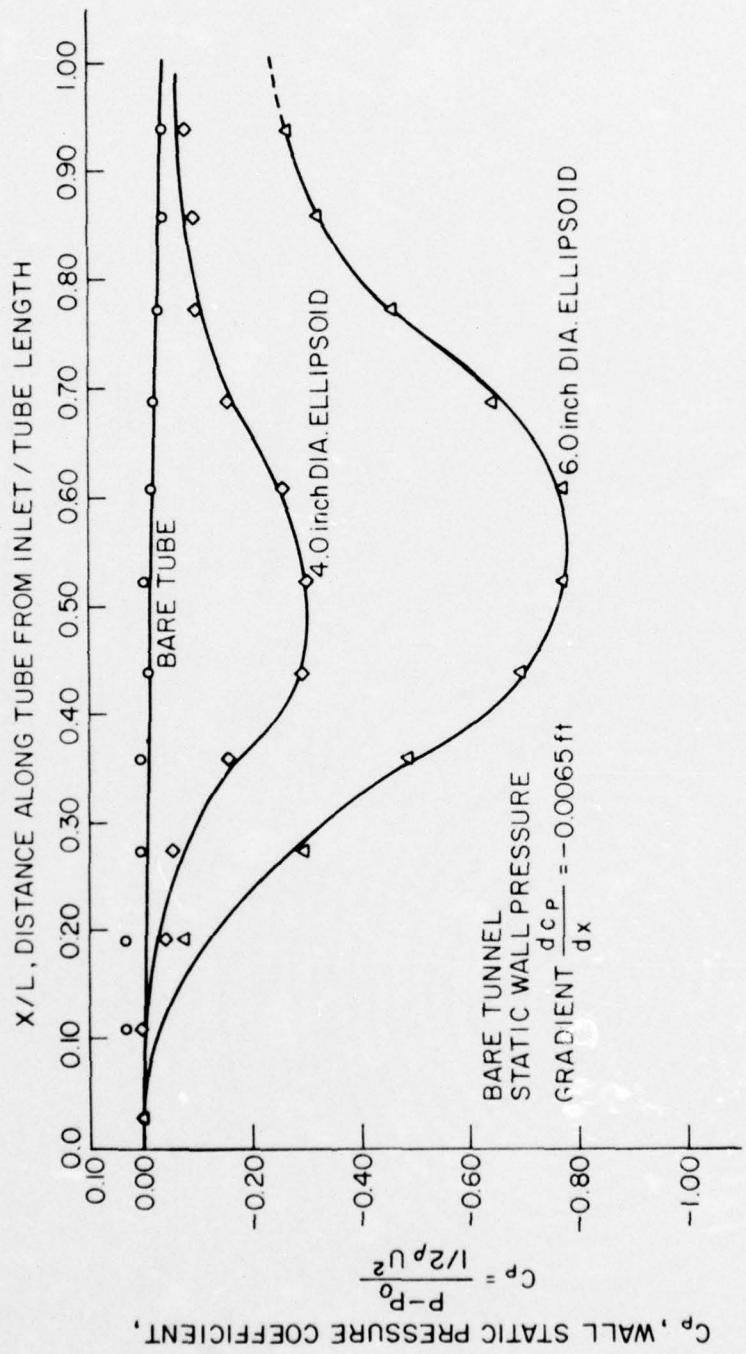
Figure 13 Static Wall Pressures in the Tube as a Function of Distance from the Tube Inlet

Figure 14  The Ellipsoids-of-Revolution

in pitching moment coefficients. Secondly, since the ultimate goal for

these tunnel corrections is the correction of water tunnel data, where

Reynolds numbers of the order of 10 times the maximum $2.3 \times 10^6$ of

the 6.0 in. diameter ellipsoid tested here are common, it was desirable

to insure that the flow over the body was indeed turbulent. Also,

even if at a later date, it was shown that no effective Reynolds number

corrections were required, $2.3 \times 10^6$ is approximately the critical

Reynolds number for the ellipsoids.

The ellipsoids were supported at their center-of-gravity by a

single 0.375-inch diameter rod manufactured of 416 stainless steel,

Figure 15. At the model end of this support rod, machining produced a

hollow thin-walled section with a 0.012 inch wall thickness approximately

1.0 inch long. To this hollow section, or torque tube, was epoxied a

threaded fitting for attachment to the ellipsoids. The design of this

torque tube and model mounting arrangements in the 4.0 inch and 6.0

inch diameter ellipsoids was such that the center of the torque tube and

the ellipsoid centerlines were coincident. This was done to minimize

any unwanted lift and drag interactions in the moment measuring system.

Unfortunately, in the 2.0-inch diameter ellipsoid, space limitations

prevented maintaining this arrangement. However, the displacement of

the torque tube center, where the electro-mechanical strain gages[34]

were placed from the 2.0-inch diameter ellipsoid centerline was held to

0.50 inches. The other end of the support rod was threaded, permitting

mounting through an adapter to an existing ARL streamlined strut.

Threading the adapter end permitted height and angle adjustments of the
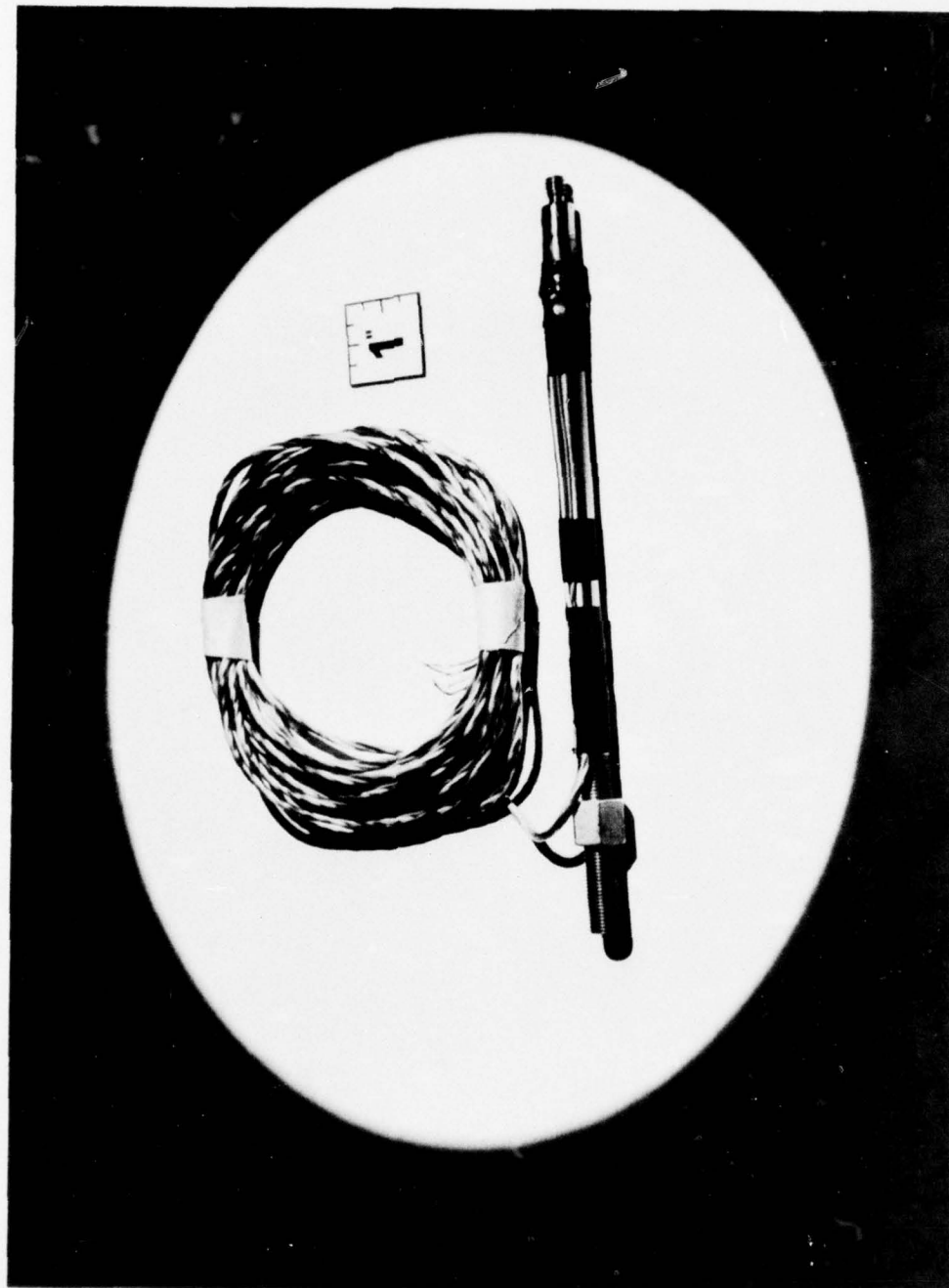
Figure 15  The Model Support Strut and Instrumented Torque Tube

model. This support rod and strut were bolted to the wind tunnel balance which was used to change the body angle of attack. The total model support moment measuring system is shown in Figure 16.

The moment measuring system or torque cell consisted of electro-mechanical strain gages placed at 45 degrees to tube axis and centered on the 1.0 inch torque tube to measure strains produced by torques applied to the tube. A basic four-arm 120 ohm strain gage bridge was used to minimize temperature effects.

## Calibrations and Velocity Measurements

A schematic of the instrumentation used for the wind tunnel tests is shown in Figure 17. The torque cell was designed to operate at a supply voltage of 5.00 volts and variable gains of either 100 or 1000. To eliminate any unwanted effects due to the strain gage power supply and amplifier, the units to be used in the actual wind tunnel testing were assembled, and the torque cell, power supply and amplifier calibrated as a system.

To calibrate the torque cell, a fixture, mounting on the torque tube in the same manner as the ellipsoids in Figure 16, with accurate moment arms of -6.0, 0.0 and 6.0 inches and applying the loads through the torque tube center, was built. By clamping the strut adaptor plate, model support rod, and calibration fixture to a vertical wall, known moments could be produced by hanging weights at the various moment arm distances. Although it was realized that loading in this manner did not produce a pure moment, but also resulted in a bending force being applied to the torque cell, loading at the zero length moment arm over
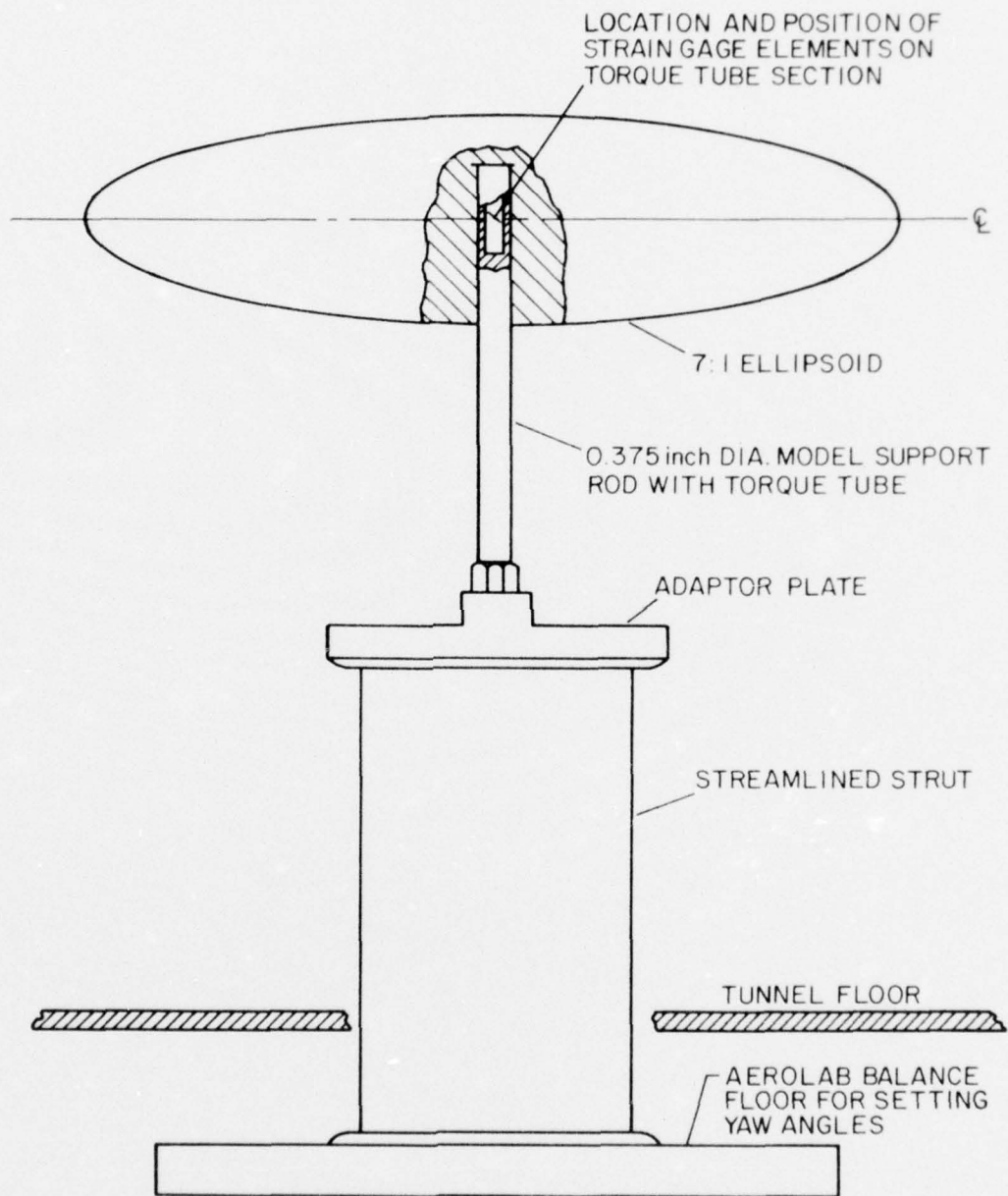
Figure 16  The Schematic of the Total Model Support System
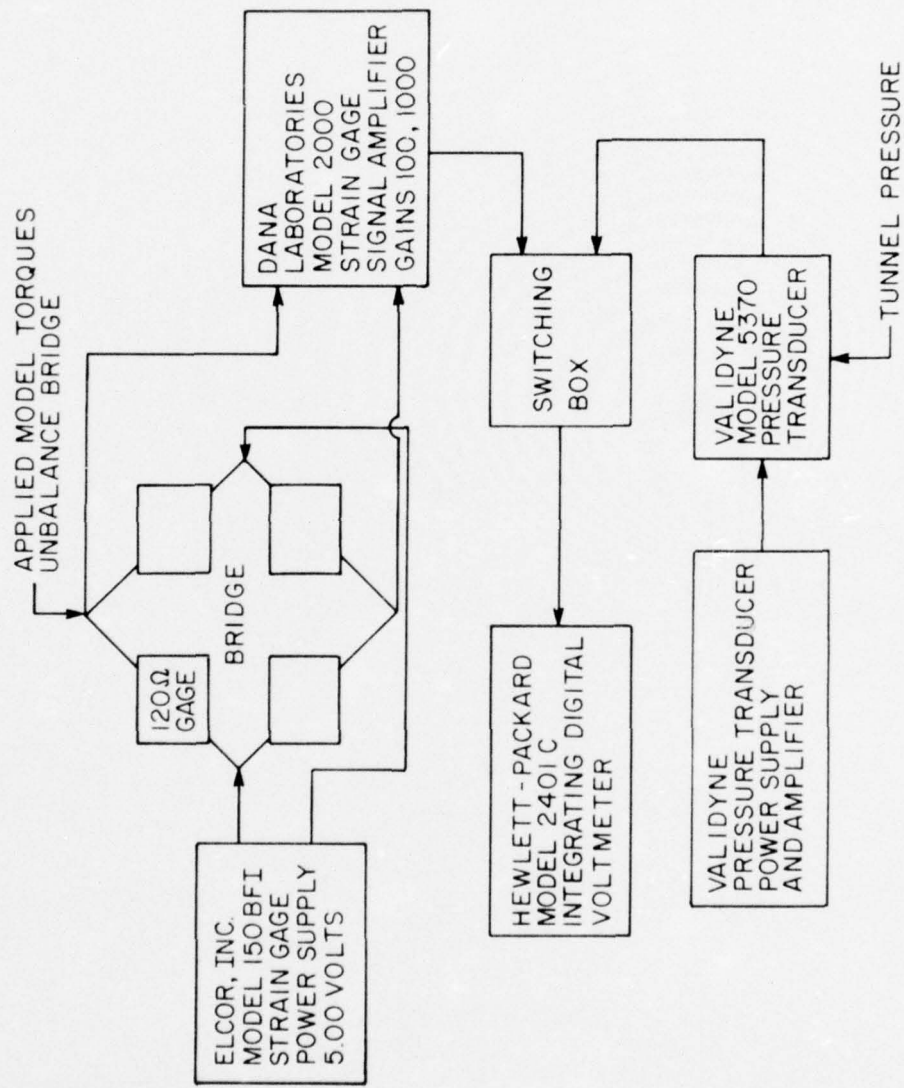
Figure 17  The Instrumentation Schematic for the Pitching Moment Tests

the calibration range produced no measurable torque interaction.
Rotating the torque cell 90.0 degrees, and repreating this test indicated
there was no torque interaction due to bending forces for all angular
orientations of the tube. The torque cell calibration was then
obtained by placing a total of 5.0 lbs. at the 6.0 inch moment arm
distance in 0.50 and 1.00 lb. increments. The resulting calibration
was 0.06026 in. lbs./MV at an amplifier gain of 100. Repeating the
calibration for an amplifier gain of 1000 resulted only in shifting
the calibration constant decimal point.

Since it was realized that the torque tube would twist, thus
changing the ellipsoid angle of ttack, dial displacement indicators
were placed at the -6.0 inch and zero moment arm distances and the
twist measured at 0.0275 deg/in. lb. This constant was used to modify
the ellipsoid angle-of-attack set with the wind tunnel balance in the
data reduction. Also, the calibration was repeated without the dial
indicators, since it was felt they might modify the calibration.
However, no measurable change in the calibration was seen due to the
presence of the dial indicators in the calibration set-up.

Since all the non-dimensional coefficients derived from tunnel
testing use velocity as a basis for calculation, one of the more
important measurements was the test section velocity. Fortunately, the
average velocity through the test section is one of the easiest of
measurements. However, the velocity in the tube, especially when a
model is installed, varies significantly from the tunnel test section
velocity as can be seen from Figure 18. The proper velocity for the
reduction of the in-tube pitching moment data to coefficient form is the
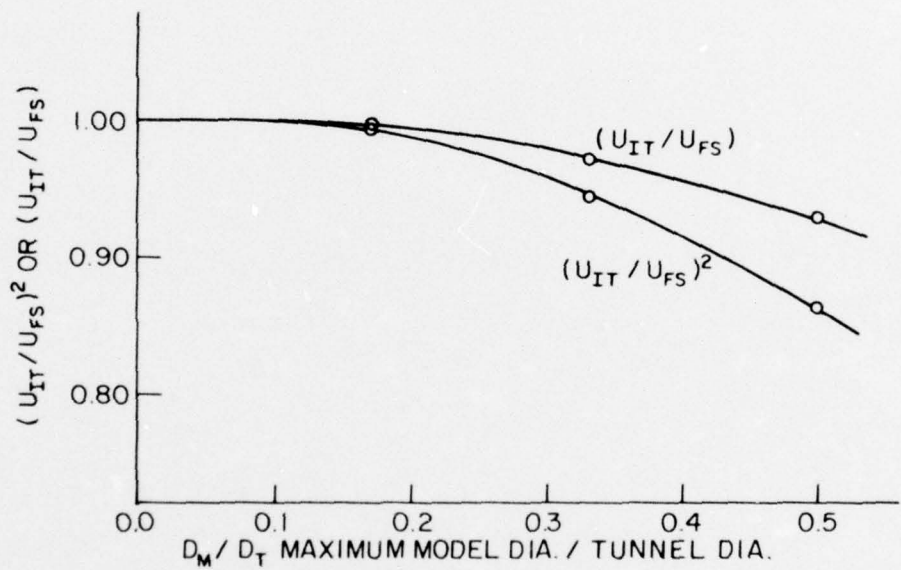
Figure 18   Dynamic Head Losses at the Tube Inlet as a Function of
Model-to-Tunnel Diameter Ratio

velocity in the tube inlet. To obtain the tube velocity, a pitot-static
probe was placed on the tube centerline approximately 3.0 inches aft
of the inlet. A second pitot-static probe was placed at the tunnel
test section throat to obtain the tunnel velocity for reduction of
the unrestricted medium pitching moment data. Figure 18 shows the
ratio of the readings from these two pitot-static probes. Periodic
comparison of the total pressures from these two pitot-static probes
insured correct velocity measurements.

All the pressure measurements, i.e., the in-tube and unrestricted
medium velocity, and the wall static pressures, were made using a
Validyne, Model 5370, pressure transducer. The calibration constant
for the particular transducer used was 1.516 inch of water/volt at a
span setting of 7.0. The span setting is a combination of transducer
supply voltage and amplifier gain.

## Test and Data Reduction Procedures for the Pitching Moment Measurements

Because of the ease with which yaw angles could be set using
the permanent wind tunnel balance the pitching moment measurements
were made in a horizontal plane. After crudely centering the ellipsoid
in the tube with the aid of a centering guide, the torque cell was
zeroed at a fixed tunnel velocity with the model at a zero angle of
attack. The centering guide consists of a plexiglass disk of diameter
equal to the diameter of the tube with cross hairs inscribed at the
center. It was realized that due to errors in the initial positioning
of the ellipsoids, a slight angle of attack and hence a small pitching
moment would exist. As only the slope of the pitching moment curve
was of interest, the change in pitching moment due to angle of attack

was measured. After zeroing the torque cell at a test velocity, the ellipsoid was rotated through a total angle of attack of 4.0 degrees in 0.5 degree increments and measurements taken at each step. A similar procedure was followed for negative angles up to -1.0 degrees. Where feasible, the procedure was repeated for several Reynolds numbers. A similar test procedure was followed for testing in the unrestricted medium.

In both cases, the data reduction followed the nondimensionalization practices outlined in Appendix A. The pitching moment coefficient $C_M$ is

$$C_M = \frac{M}{1/2\rho\ U^2 S_M \ell} \quad . \tag{52}$$

Also, allowances were made in the data reduction for the increased angles-of-attack due to twisting of the torque tube under the applied pitching moments.

## Results of the Pitching Moment Experiments

Figures 19, 20, 21 are typical plots of the measured pitching moment coefficients as a function of angle of attack for the various ellipsoids, both in the unrestricted medium and in the tube. Figure 22 is a composite plot of all the experimental data.

A series of tests, primarily with the 6.0 inch diameter ellipsoid, Figure 21, were conducted to assess the effects of Reynolds number on the pitching moment coefficient. Over the modest Reynolds number
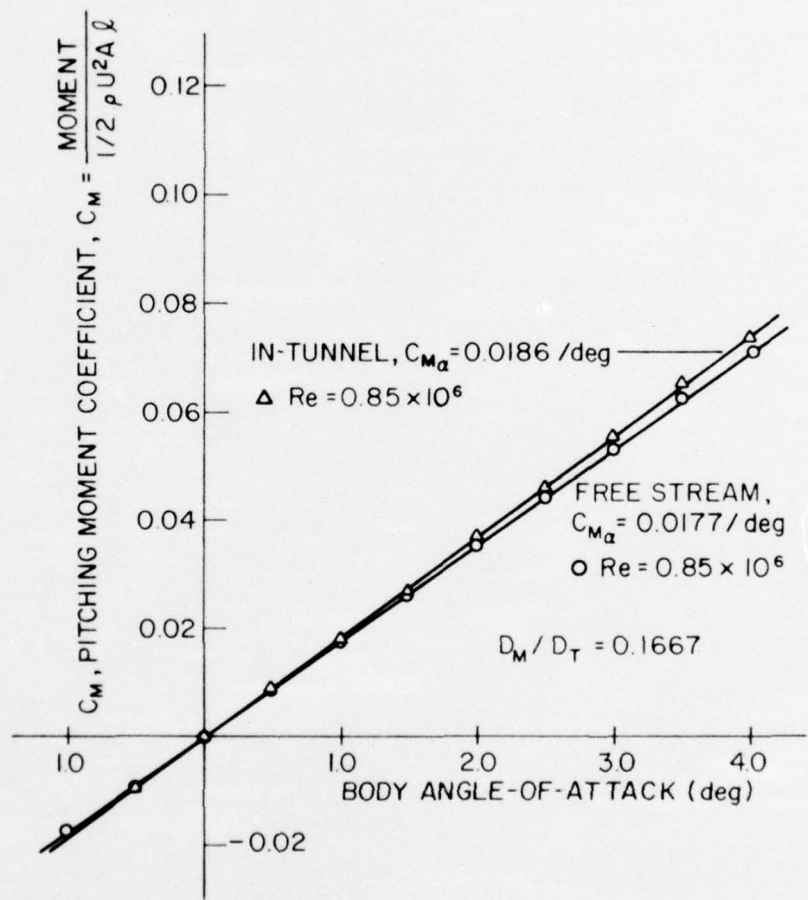
Figure 19 Static Pitching Moment Coefficient as a Function of the
Body Angle of Attack: 2.0-in.-Diameter Ellipsoid
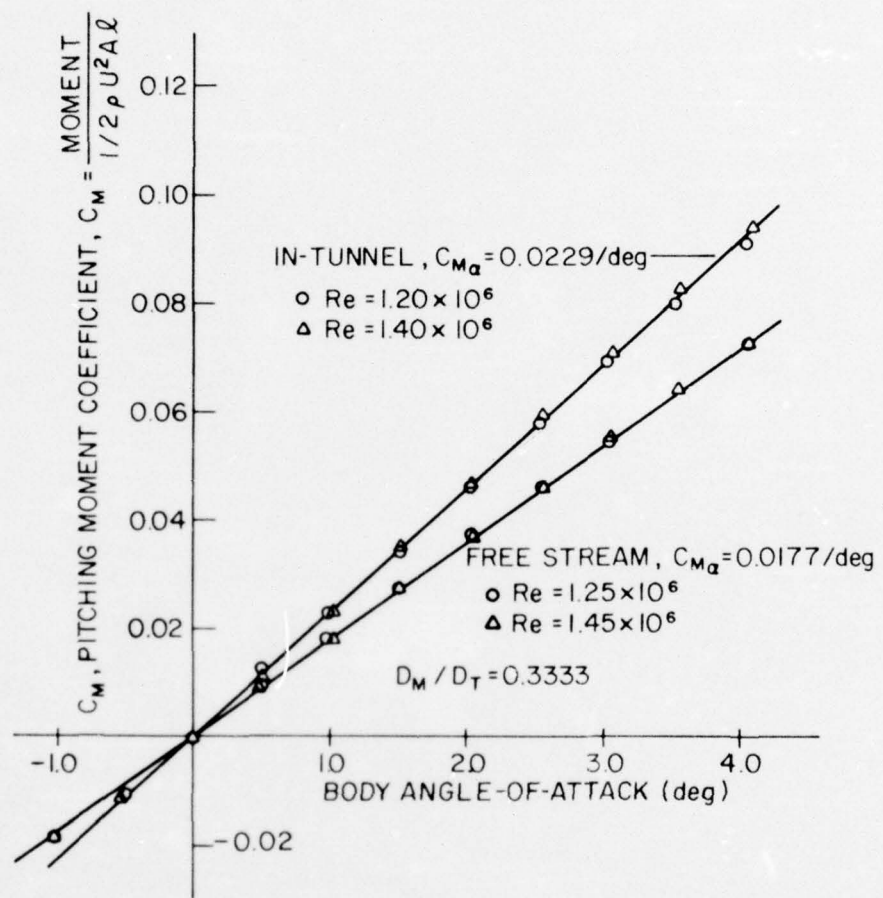
Figure 20   Static Pitching Moment Coefficient as a Function of the
Body Angle of Attack:  4.0-in.-Diameter Ellipsoid
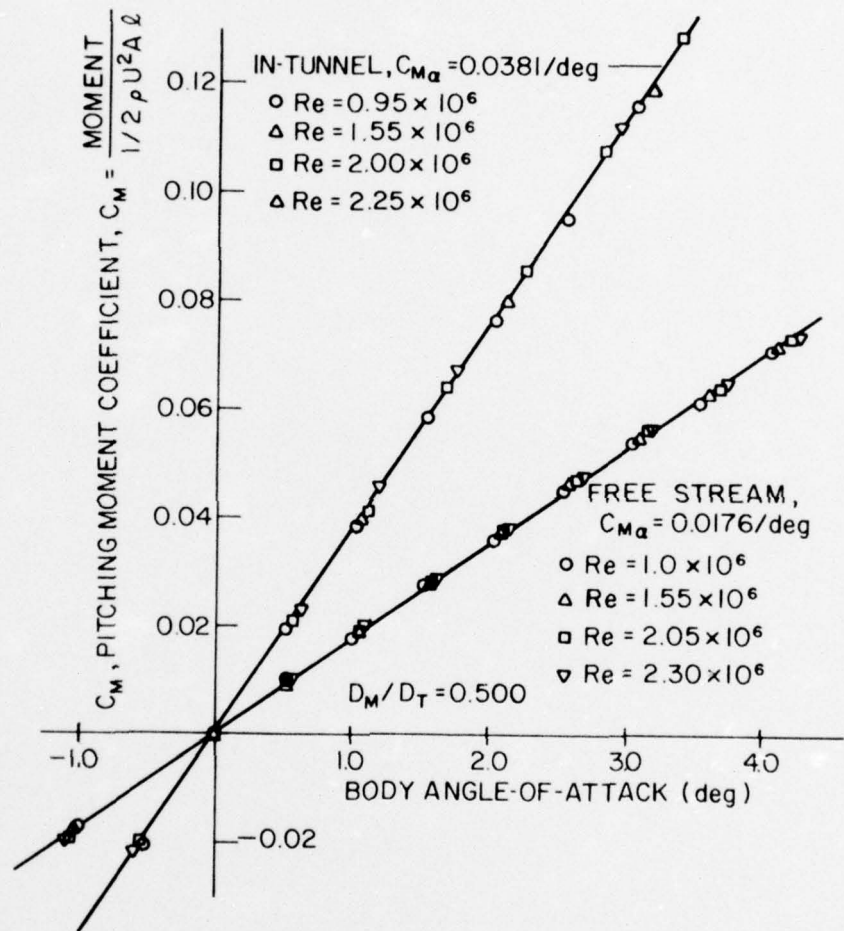
Figure 21   Static Pitching Moment Coefficient as a Function of the
Body Angle of Attack:   6.0-in.-Diameter Ellipsoid
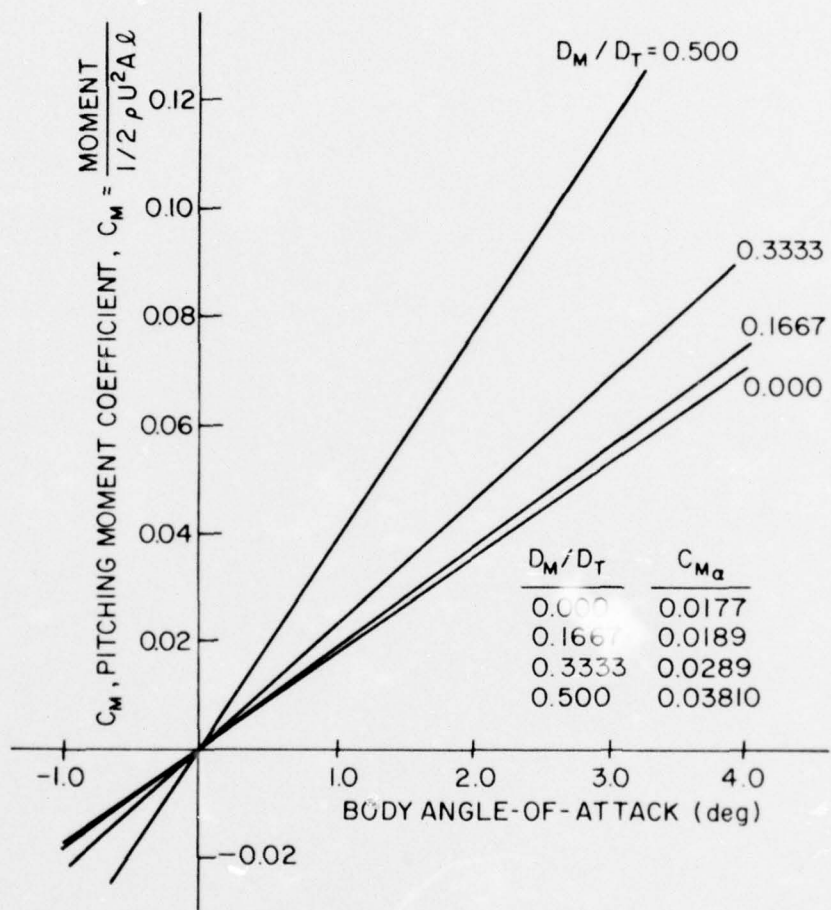
Figure 22    Pitching Moment Coefficients as a Function of the
Body Angle of Attack:   All Ellipsoids

range available, there was no measurable effect on the body pitching

moment coefficient due to Reynolds number.

In addition, it has been expected that using the common model

support strut of Figure 15, for all the ellipsoids would result in

varying degrees of model-strut interference on the pitching moment

coefficients. This model-strut interference would have been expected

to be a function of the model-to-strut diamter ratio, and to be

evidenced by significant changes in the pitching moment coefficient

slope, $C_{M_\alpha}$ , in the unrestricted medium tests of the three ellipsoids.

However, this was not the case; the unrestricted medium $C_{M_\alpha}$ being

essentially constant for all three ellipsoids tested. These tests do

not preclude a constant model-strut interference correction to $C_{M_\alpha}$ ,

evaluation of which would require additional testing with a second

dummy strut to restore symmetry. It does appear that such a model-strut

correction would be a constant multiplication factor for all three

ellipsoids. As such, a multiplicative model-strut interference

correction to the pitching moment coefficient slope, $C_{M_\alpha}$ would not

affect the experimental tunnel wall interference correction for $C_{M_\alpha}$ .

Appendix C develops the reasoning behind this statement.

Table II collects the experimental pitching moment coefficient

slope data and defines the experimental tunnel interference correction

for $C_{M_\alpha}$ . In defining the experimental $C_{M_\alpha}$ correction, it was

assumed that a $\pm$ 1.0 percent error in graphically defining $C_{M_\alpha}$ from

TABLE II

TABULATED PITCHING MOMENT COEFFICIENT SLOPES AND TUNNEL INTERFERENCE CORRECTIONS

| MODEL | MODEL/TUNNEL DIAMETER RATIO | $C_{M_\alpha}$ (MINIMUM) | $C_{M_\alpha}$ (AVERAGE) | $C_{M_\alpha}$ (MAXIMUM) | MINIMUM CORRECTION | AVERAGE CORRECTION | MAXIMUM CORRECTION |
|---|---|---|---|---|---|---|---|
| ALL MODELS | 0.00 | 0.0175 | 0.0177 | 0.0179 | 0.978 | 1.00 | 1.022 |
| 2.0-INCH-DIAMETER ELLIPSOID | 0.1667 | 0.0184 | 0.0186 | 0.0188 | 1.024 | 1.053 | 1.082 |
| 4.0-INCH-DIAMETER ELLIPSOID | 0.333 | 0.0227 | 0.0229 | 0.0231 | 1.261 | 1.293 | 1.326 |
| 6.0-INCH-DIAMETER ELLIPSOID | 0.500 | 0.377 | 0.0381 | 0.0385 | 2.106 | 2.153 | 2.203 |

NOTE: In defining $C_{M_\alpha}$ from Figures 19, 20, and 21 for the various models, it is assumed that there can be a $\pm 1.0$ percent error in graphical determination of the slopes. This $\pm 1.0$ percent corrections following Equation (53). slope error is used to define the minimum and maximum $C_{M_\alpha}$

the plots, Figures 19, 20, and 21 was possible. Then, three experimental $C_{M_\alpha}$ model/tunnel interference corrections were defined at each model-to-tunnel diameter ratio. They are:

(1) The maximum correction

$$\frac{C_{M_{\alpha_{IT}}} \text{(Maximum)}}{C_{M_{\alpha_{FS}}} \text{(Minimum)}}$$

(2) The minimum correction

$$\frac{C_{M_{\alpha_{IT}}} \text{(Minimum)}}{C_{M_{\alpha_{FS}}} \text{(Maximum)}} \qquad (53)$$

and

(3) The average correction

$$\frac{C_{M_{\alpha_{IT}}} \text{(Average)}}{C_{M_{\alpha_{FS}}} \text{(Average)}}$$

These experimental $C_{M_\alpha}$ tunnel wa-1 interference corrections for $C_{M_\alpha}$ are plotted with the theoretical predictions on Figure 9 for comparison.

Semi-empirical predictions[27] of the pitching moment coefficient slope, $C_{M_\alpha}$, for the ellipsoids indicate a value of 0.0188/degree in the unrestricted medium. The experimentally determined value for $C_{M_\alpha}$ averaged 0.0177/degree or approximately 5.8 percent below the empirical value. Aside from a possible constant model-strut interference correction, Appendix C provides an analysis of the possible errors in the measurements of $C_M$.

As an aid to future researchers, attempting to duplicate the experimental results of this thesis, the experimental data used to generated  Figures 19 to 22  are tabulated as Appendix D.

CHAPTER VI

SUMMARY AND CONCLUSIONS

The results of the theoretical and experimental work contained in this thesis are summarized by Figures 9 and 10. One must conclude from Figure 9 that the present theory developed from slender body theory is inadequate for predicting corrections to $C_{M_\alpha}$ and $C_{L_q}$ for tunnel wall interference. The possible exception to this statement might be the correction to experimental $C_{M_\alpha}$ and $C_{L_q}$ data for models with a model to tunnel diameter ratio of less than approximately 0.20. Here, the uncertainties in the experimental data presented in Table 2 and Appendix C make a decision between the various theories difficult. However, based on the average experimental correction for $C_{M_\alpha}$, the theories of Goodman or Peirce, appear to agree better with the experimental results than the present theory. Unfortunately, no similar statements regarding the applicability of any of the three theories discussed in this thesis for correcting the experimental acceleration stability derivatives $C_{L_{\dot\alpha}}$ and $C_{M_{\dot q}}$, for tunnel wall interference can be made since no experimental data exists for comparison.

Goodman's theory appears to offer the best agreement with the present experimental $C_{M_\alpha}$ interference correction data in a model-to-tunnel diameter ratio range of practical interest. The upper limit for this

range is a model-to-tunnel diameter ratio of approximately 0.40.

However, for the differences between the interference corrections for

$C_{M_\alpha}$ as predicted by Goodman or Peirce, the computational complexity of

Goodman's technique makes Peirce's simple theory look very attractive

for rough or preliminary calculations. Also, the present experimental

interference correction data for $C_{M_\alpha}$ departs from Goodman's theory

for the higher model-to-tunnel diameter ratios and approaches Peirce's

theory. Further pitching moment measurements at model to tunnel

diameter ratios between 0.40 and 0.50 are needed to establish the tunnel

interference correction in this range of model to tunnel diameter ratios.

Since in the range of practical model-to-tunnel diameter ratios

below approximately 0.40 Goodman's theory offers the best overall

agreement with the limited experimental data of this thesis and does

consider the effect of body geometry on the interference corrections,

it is suggested that all future theoretical work involve this theory.

However, the theory developed for this thesis may prove useful in

indicating relative effects of body shape parameters such as prismatic

coefficient or body cross-sectional area distributions on the tunnel

interference corrections.

The concept of the interference correction developed for this

thesis is uniquely suited for correcting the experimental stability

derivative data obtained from testing with the Planar Motion Mechanism.

For Planar Motion Mechanism tests, the flow-correcting liner technique

developed by Peirce for correcting pressure distributions on the body

has several disadvantages. First, the liner is only good for cases
where the body is axisymmetric in the tunnel. Obviously, for cases
where the body is at an angle of attack or displaced from the tunnel
centerline by the oscillations of the Planar Motion Mechanism, the
flow-correcting liner is not correct. Indeed, to use the flow-correcting
liner for bodies at an angle of attack would require a different liner
for each angle of attack. The ocst in time and materials make this
approach impractical. Secondly, although the liner does provide an
approximately correct pressure distribution over the body, the accuracy
of the correction provided by the liner is not sufficient for drag
measurements. This is evidenced by the need for further corrections
to experimental drag measurements made in the 48.0-inch-diameter water
tunnel at ARL.

# CHAPTER VII

## RECOMMENDATIONS FOR FURTHER RESEARCH

This thesis has presented tunnel interference corrections for
only one prismatic coefficient and body cross-sectional area
distribution, namely the ellipsoid.  It would prove interesting to
examine the effect of varying the model cross-sectional area
distributions on the body x-axis at the prismatic coefficient of the
ellipsoid, using Goodman's theory for the tunnel interference corrections
as a practical minimum.  Similarly, varying the prismatic coefficient
and the body cross-section area distribution would establish the theory
sensitivity to body geometry.  In the limit as the prismatic coefficient,
$\gamma$  approaches 1.0 Goodman's results should approach Peirce's theory,
Equation (2).

In light of the magnitude of the uncertainties possible in the
experimental correction factor data further static pitching moment
experiments, attempting to distinguish subtle variations in body
geometry appear futile.  One exception to further testing would be
further static pitching moment tests of an ellipsoid with a model to
tunnel diameter ratio of approximately 0.42 to confirm the departure

of the experimental correction from Goodman's theory at the higher

model to tunnel diameter ratios. Also, no experimental verification

of the tunnel interference corrections for the acceleration stability

derivatives of Figure 10 has been offered. Finally, further theoretical

and experimental work yielding tunnel interference corrections for

$C_{L_\alpha}$ would be useful.

References

1. Peirce, T. E., "Tunnel Wall Interference Effects on the Drag and Pitching Moment of an Axisymmetric Body", Ordnance Research Laboratory, TM 501.8871-02, January, 1964.

2. Goodman, T. R., "Aerodynamic Characteristics of a Slender Body Traveling in a Tube", AIAA Journal, Vol. 9, No. 4, April, 1971, pp. 712-717.

3. Etkin, B., Dynamics of Flight, John Wiley and Sons, Inc., New York, New York, 1965.

4. Brownell, W. F., "A Rotating-Arm and Maneuvering Basin," DTMB Report 1053, 1953.

5. Price, D. A., "Free-Body Modeling of the Dynamics of a Fin Stabilized Ballistic Missile in Non-Spinning Vertical Trajectories", Hydroballistics Laboratory Report E-73-1, April, 1957.

6. Caster, H. P., "Hydrodynamic Trajectory Computations and Analyses for Horizontally-Launched Rounds of the Basic Finner Missile", NPG Report No. 1668, August 15, 1959.

7. Kiceniuk, T., "An Experimental Determination of Dynamic Coefficients for the Basic Finner Missile by Means of the Angular Dynamic Balance", CIT Report E-73-3, June, 1957.

8. Kiceniuk, T., "An Experimental Determination of Dynamic Coefficients for the Basic Finner Missile by Means of the Angular Dynamic Balance", CIT Report E-73-3, June, 1957.

9. Gertler, M., "The DTMB Planar Motion Mechanism System", NSRDC Report 2523, July, 1967.

10. Goodman, A., "Experimental Techniques and Methods of Analysis Used in Submerged Body Research", Third Symposium on Naval Hydrodynamics, 19-21, September, 1960.

11. Lehman, A. F., "The Garfield Thomas Water Tunnel", Ordnance Research Laboratory External Report, Serial No. NOrd 16597-56, September, 1959.

12. Hall, W. R., "The ORL Planar Motion Mechanism (PMM) - Theoretical Considerations", Ordnance Research Laboratory TM 72-10, January, 1972.

13. Dugoff, M., "Predictions of Trajectories for an Underwater Missile", Stevens Institute of Technology, DL Report No. 989, February, 1963.

14. Pope, A. and J. Harper, Low-Speed Wind Tunnel Testing, John Wiley and Sons, Inc., New York, New York, 1966.

15. Munk, M. M., "The Aerodynamic Forces on Airship Hulls", NACA TR 184, January, 1924.

16. Abbott, I. H., "Airship Model Tests in the Variable Density Wind Tunnel", NACA TR 394, January, 1931.

17. Freeman, "Pressure Distribution Measurements on the Hull and Fins of a 1/40-Scale Model of the U. S. Airship 'Akron'", NACA TR 443, June, 1932.

18. Upson, R. H. and W. A. Klikoff, "Application of Practical Hydrodynamics to Airship Design", NACA TR 405, June, 1931.

19. Glauert, H., "The Interference of a Wind Tunnel on a Symmetrical Body", Air Research Committee (British) R and M 1544, May, 1933.

20. "Aerodynamic Characteristics of a Body Traveling in a Tube", NASA Literature Search No. 18209, March, 1972.

21. Sprieter, J. R., "The Aerodynamic Forces on Slender Plane and Cruciform Wing Body Combinations", NACA TR 962, March, 1949.

22. Ribner, H. S., "The Stability Derivatives for Low-Aspect-Ratio Triangular Wings at Subsonic and Supersonic Flows", NACA TN 1423, September, 1947.

23. Hoffman, G. H., and M. H. Platzer, "On Supersonic Flow Past Oscillating Bodies of Revolution", AIAA Journal, Vol. 4, No. 2, February, 1966, pp. 370-371.

24. Smith, A. M. O. and J. L. Hess, "Calculation of the Potential Flow About Arbitrary Bodies", Progress in the Aeronautical Sciences, Vol. 8, Pergamon Press, New York, New York, 1966.

25. Newman, J. N., "The Force and Moment on a Slender Body of Revolution Moving Near a Wall", DTMB Report No. 2127, December, 1965.

26. Levine, P., "Incompressible Potential Flows About Axially Symmetric Bodies in Ducts", Journal of the Aerospace Sciences, Vol. 25, No. 1, January, 1958, pp. 33-36.

27. Segel, L. A., "Application of Conformal Mapping to Viscous Flow Between Moving Circular Cylinders", Quarterly of Applied Mathematics, Vol. XVIII, No. 4, 1961, pp. 335-353.

28. Jones, R. T., "Properties of Low-Aspect-Ratio Pointed Wings at Speeds Below and Above the Speed of Sound", NACA TR 835, May, 1945.

29. Adams, M. C. and W. R. Sears, "Slender Body Theory: Review and Extension", Journal of the Aeronautical Sciences, Vol. 20, February, 1953, pp. 85-98.

30. Allen, H. J. and E. W. Perkins, "A Study of the Effects of Viscosity on Flow Over Slender Inclined Bodies-of-Revolution", NACA TR 1048, 1951.

31. Abkowitz, M. A. and D. L. Paster, "Hydrodynamic Stability and Control Derivatives", U. S. Naval Underwater Ordnance Station, TM 120, February, 1957.

32. Davis, R. F., "Spline Curve Fit Functions, Their Derivation and Use", Ordnance Research Laboratory TM 512.3531-02, July, 1968.

33. Nielsen, K. L., Methods in Numerical Analysis, MacMillan Co., New York, New York, 1956.

34. Gurney, G. B., "An Analysis of Force Measurement", M. S. Thesis, The Pennsylvania State University, 1962.

35. Wendel, K., "Hydrodynamic Masses and Hydrodynamic Moments of Inertia", DTMB Transl. No. 260, July, 1956.

APPENDIX A

NON-DIMENSIONALIZATION PRACTICES

Equations (9), (26), (29), (30), and (31) are non-dimensionalized using the unblocked tunnel or free stream velocity, U, the body length, $\ell$ ; and the maximum cross-sectional area of the body, $S_M$. A dimensionless time $\bar{t}$ is defined such that

$$t = \frac{\ell}{U} \bar{t} \tag{A-1}$$

and

$$\frac{d}{dt} = \frac{U}{\ell} \frac{d}{d\bar{t}} \qquad . \tag{A-2}$$

Then, it follows

$$
\begin{array}{lll}
L = 1/2 \ \rho U^2 \ S_M C_L & \bar{\dot{h}} = \alpha & b = \bar{b}\ell \\[2ex]
M = 1/2 \ \rho U^2 \ S_M C_M & a = \bar{a}\ell & U_x = \bar{U}_x U \\[2ex]
q = \frac{U}{\ell} \bar{q} & R = \bar{R}\ell & \dot{\bar{h}} = \frac{U^2}{\ell} \dot{\alpha} \\[2ex]
q = (\frac{U}{\ell})^2 \dot{\bar{q}} & x = \bar{x}\ell & \dot{\alpha} = \frac{U}{\ell} \bar{\dot{\alpha}}
\end{array}
\tag{A-3}
$$

where an overbar indicates a non-dimensional quantity. $C_L$ and $C_M$ are the non-dimensional lift and pitching moment coefficients, respectively, and may be written in the form of Equation (1), in terms of $\alpha$, $\bar{\dot{\alpha}}$, $\bar{q}$, or $\bar{\dot{q}}$, leading to the non-dimensional stability derivatives.

APPENDIX B


A GENERAL BERNOULLI EQUATION FOR A MOVING COORDINATE SYSTEM


The following development for the pressures produced in steady
and unsteady translational motion in a two-dimensional field of flow
is due to Wendel[35]. Consider a liquid particle whose center is
assumed to lie at the point z, y at time t. At time $t + \delta t$, the
same particle is located at the point $z + wdt$, $y + vdt$, where the
velocities in the z and y directions are designated by w and v,
respectively. Furthermore, let P equal the pressure, $\rho$ the
density, Z and Y the components of the external forces per unit
length at the point (z, y) at time t and $\delta z$ and $\delta y$ the lengths of
the elements. In order to use the velocity potentials, Equations (18)
and (19), which refer to a cylinder moving in a stationary medium, a
coordinate system which moves with the cylinder is required. In that
case, the change of position of the particle with respect to the
moving system is $(w - \dot{Z}_o)$ in the Z direction. Then, summing forces
on the fluid element in the z and y directions and simplifying
obtain:

$$\frac{dw}{dt} + (w - \overset{\circ}{Z}_o) \frac{dw}{dz} + v \frac{dw}{dy} = Z - \frac{1}{\rho} \frac{dP}{dz}$$

and                                                                                    (B-1)

$$\frac{dv}{dv} + (w - \overset{\circ}{Z}_o) \frac{dv}{dz} + v \frac{dv}{dy} = Y - \frac{1}{\rho} \frac{dP}{dy} \quad .$$

which are Euler's equations referred to a coordinate system moving in translation with velocity $\overset{\circ}{Z}_o$ . The assumed ideal fluid has a velocity potential; hence, the following apply:

$$w = \frac{d\phi}{dz} \qquad v = \frac{d\phi}{dy} \quad ,$$

and thus, also,    $\dfrac{dw}{dy} = \dfrac{d^2\phi}{dy\,dz} \qquad \dfrac{dv}{dz} = \dfrac{d^2\phi}{dy\,dz}$                        (B-2)

The external and hydrostatic forces need not to be considered any further, since the investigations concern only dynamic forces. Introducing Equations (B-2) into Euler's equations, Equation (B-1) yields

$$\frac{d^2\phi}{dz\,dz} + (w - \overset{\circ}{Z}_o) \frac{dw}{dz} + v \frac{dv}{dz} = -\frac{1}{\rho} \frac{dP}{dz}$$

and                                                                                    (B-3)

$$\frac{d^2\phi}{dy\,dt} + (w - \overset{\circ}{Z}_o) \frac{dw}{dy} + v \frac{dv}{dy} = -\frac{1}{\rho} \frac{dP}{dy} \quad .$$

The Bernoulli Equation arises from the integration of Equation (B-3). For the purposes of integration note that

$$\frac{1}{2} \frac{d}{dz} (w^2) = \frac{1}{2} \frac{d}{dw} (w^2) \frac{dw}{dz} = w \frac{dw}{dz} \qquad (B-4)$$

and that Equation (B-3) may be written:

$$\frac{d}{dz} \left\{ \frac{d\phi}{dt} + \frac{1}{2} (w^2 + v^2) - w\dot{Z}_o \right\} = -\frac{d}{dz} \left[ \frac{P}{\rho} \right]$$

and                                                                    (B-5)

$$\frac{d}{dy} \left\{ \frac{d\phi}{dt} + \frac{1}{2} (w^2 + v^2) - w\dot{Z}_o \right\} = -\frac{d}{dy} \left[ \frac{P}{\rho} \right] .$$

Performing the indicated integration, obtained from each of these Equations (B-5), the following relationship.

$$\frac{d\phi}{dt} + \frac{1}{2} (w^2 + v^2) - \dot{Z}_o w + \frac{P}{\rho} = F(t) , \qquad (B-6)$$

where the integration constant, $F(t)$ may still be a function of $t$. Equation (B-6) may be designated as a general Bernoulli equation for a coordinate system moving with a velocity $\dot{Z}_o$. In the polar coordinates of Figure 4, Equation (B-6) may be written:

$$\frac{d\phi}{dt} + \frac{1}{2} \rho (\phi_r^2 + \frac{1}{r^2} \phi_\theta^2) - \dot{Z}_o (\phi_r \cos \theta - \frac{1}{r} \phi_\theta \sin \theta) + \frac{P}{\rho} = F(t)$$

$$(B-7)$$

where

$$\phi_r = \frac{\partial \phi}{\partial r} \quad , \quad \text{the radial velocity component}$$

$$\frac{1}{r} \phi_\theta = \frac{1}{r} \frac{\partial \phi}{\partial \theta} \quad , \quad \text{the angular velocity component.}$$

APPENDIX C

ERROR ANALYSIS FOR THE PITCHING MOMENT DATA

The errors in any measurement may be classified into two categories: constant and random. Constant errors, such as calibration and gain errors influence the magnitude of the data, while random errors, such as the reading fluctuations, reflect the precision and accuracy of the reading instrumentation.

Since a common measurement system was used for all measurements, the constant errors should be of no importance for the relative comparison of Table II. That is, the pitching moment coefficient, $C_M$ may be written

$$C_M = K(V_1/V_2) , \qquad (C-1)$$

where  K =  combination of model cross-sectional area, body length,
            torque and pressure transducer calibrations,

       $V_1$ =  output from torque tube, and

       $V_2$ =  output of the pressure transducer.

Then, for the experimental interference correction for  $C_{M_\alpha}$ , defined as the ratio of  $C_{M_\alpha}$  for the body in the tunnel so that for body in the unrestricted medium.

$$\frac{C_{M_{IT}}}{C_{M_{FS}}} = \frac{C_{M_{\alpha_{IT}}}}{C_{M_{\alpha_{FS}}}} = \frac{(V_1/V_2)_{IT}}{(V_1/V_2)_{FS}} \qquad (C-2)$$

Therefore, magnitude errors will not affect the relative comparisons.

Errors over which the experimenter has no control or random errors such as temperature and pressure fluctuations, calibration precision, and instrumentation accuracy and linearity, affect the degree of confidence which can be placed in the experimental data.

The first random error considered is that of the torque tube calibration. In the calibration apparatus, the moment arm had a precision of $\pm 0.005$ in. while the weights were accurate to $\pm 0.10$ percent. Thus, the uncertainty in applying the calibration torques was $\pm 0.18$ percent. In reading the calibration torques from the voltmeter, the maximum reading was 398 MV with an uncertainty of $\pm 0.50$ MV. Then, the total torque tube calibration uncertainty was $\pm 0.30$ percent.

Similarly, the uncertainty in the pressure transducer calibration was $\pm 0.14$ percent, thus, the total calibration error or uncertainty shown as column 1 of Table III, was $\pm 0.44$ percent.

For the rotary table, i.e., the wind tunnel balance used to set the body angles of attack, the finest readable increment was $\pm 0.10$ degree. Thus, the 4.0 degree maximum angle of attack, and an assumed uncertainty of $\pm 0.05$ degree yeilds the $\pm 1.25$ percent precision error presented as column 2 of Table III.

Column 3 of Table IV combines the uncertainties in the torque cell and pressure transducer readings as was done for the calibration precision errors. The total precision error or uncertainty in the pitching moment coefficient data, column 4 of Table III is then the sum of all the component precision estimates.

In all cases, the uncertainty in the experimental pitching moment coefficient $C_M$ is less than $\pm 2.6$ percent.

The uncertainty or precision error in the experimental $C_{M_\alpha}$ interference correction could be obtained in a manner similar to that expressed in Equation (53). Column 5 of Table III gives the precision limits on the experimental $C_{M_\alpha}$ interference correction. Note that this precision estimate compares favorably with the maximum and minimum corrections derived by assuming a $\pm 1.0$ percent error in obtaining $C_{M_\alpha}$ from a graphical determination of the slopes in Figures 19, 20, 21 and 22.

## TABLE III

### PITCHING MOMENT COEFFICIENT ERROR ESTIMATES

| MODEL | MODEL/TUNNEL DIAMETER RATIO | CALIBRATION ERRORS, PERCENT | ANGLE SETTING ERRORS, PERCENT | VOLTMETER READING ERRORS, PERCENT | TOTAL ERROR PERCENT | $C_{M_\alpha}$ CORRECTION ERRORS, PERCENT |
|---|---|---|---|---|---|---|
| ALL MODEL ELLIPSOIDS | 0.000 | ±0.44 | ±1.25 | ±0.26 - 0.65 | ±1.95 - 2.00 | ±4.00 |
| 2.0-INCH-DIA. ELLIPSOIDS | 0.1667 | ±0.44 | ±1.25 | ±0.66 | ±2.35 | ±4.40 |
| 4.0-INCH-DIA. ELLIPSOIDS | 0.3333 | ±0.44 | ±1.25 | ±0.96 | ±2.65 | ±4.70 |
| 6.0-INCH-DIA. ELLIPSOIDS | 0.5000 | ±0.44 | ±1.25 | ±0.46 | ±2.15 | ±4.20 |

NOTE: (1) Calibration error is the total error involved in torque tube and pressure transducer calibration and includes possible errors in applying torques or pressures, and uncertainties in reading the voltmeter during calibration.

(2) Voltmeter reading error is the total error involved in torque tube and pressure transducer reading during wind tunnel tests

# APPENDIX D

## TABULATED PITCHING MOMENT COEFFICIENT DATA

As an aid to future researchers attempting to duplicate the results of this thesis, the experimental $C_M$ data used to generate Figures 19 to 22 for the various ellipsoids are tabulated.

## TABLE IV

### PITCHING MOMENT COEFFICIENT DATA: 2.0-INCH DIAMETER ELLIPSOID

| $Re_{FS} \times 10^6$ | $\alpha$, DEGREES | $C_{M_{FS}} \times 10^2$ | $Re_{IT} \times 10^6$ | $\alpha$, DEGREES | $C_{M_{IT}} \times 10^2$ |
|---|---|---|---|---|---|
| 0.85 | -1.00 | -1.75 | 0.85 | -1.00 | -- |
| | -0.50 | -- | | -0.50 | -0.95 |
| | 0.00 | 0.00 | | 0.00 | 0.00 |
| | 0.50 | 0.85 | | 0.50 | 0.90 |
| | 1.00 | 1.75 | | 1.00 | 1.80 |
| | 1.50 | 2.60 | | 1.50 | 2.70 |
| | 2.00 | 3.54 | | 2.00 | 3.70 |
| | 2.50 | 4.42 | | 2.50 | 4.60 |
| | 3.00 | 5.32 | | 3.00 | 5.55 |
| | 3.50 | 6.25 | | 3.50 | 6.50 |
| 0.85 | 4.02 | 7.10 | 0.85 | 4.00 | 7.35 |

TABLE V

PITCHING MOMENT COEFFICIENT DATA: 4.0-INCH DIAMETER ELLIPSOID

| $Re_{FS} \times 10^6$ | $\alpha$, DEGREES | $C_{M_{FS}} \times 10^2$ | $Re_{IT} \times 10^6$ | $\alpha$, DEGREES | $C_{M_{IT}} \times 10^2$ |
|---|---|---|---|---|---|
| 1.25 | -1.02 | -1.80 | 1.20 | -0.50 | -1.10 |
| | 0.00 | 0.00 | | 0.00 | 0.00 |
| | 0.50 | 0.95 | | 0.50 | 1.20 |
| | 1.00 | 1.80 | | 1.02 | 2.30 |
| | 1.50 | -- | | 1.56 | 3.40 |
| | 2.04 | 3.70 | | 2.02 | 4.60 |
| | 2.54 | 4.60 | | 2.54 | 5.80 |
| | 3.56 | 6.40 | | 3.54 | 8.00 |
| 1.25 | 4.08 | 7.30 | 1.20 | 4.06 | 9.10 |
| | | | | | |
| 1.45 | -1.02 | -1.87 | 1.45 | -0.52 | -1.15 |
| | 0.00 | 0.00 | | 0.00 | 0.00 |
| | 0.50 | 0.90 | | 0.50 | 1.15 |
| | 1.04 | 1.80 | | 1.04 | 2.35 |
| | 1.52 | 2.75 | | 1.52 | 3.50 |
| | 2.04 | 3.70 | | 2.04 | 4.70 |
| | 2.56 | 4.62 | | 2.56 | 5.95 |
| | 3.06 | 5.55 | | 3.08 | 7.10 |
| | 3.56 | 6.40 | | 3.58 | 8.30 |
| 1.45 | 4.08 | 7.30 | 1.45 | 4.10 | 9.40 |

TABLE VI

PITCHING MOMENT COEFFICIENT DATA:  6.0-INCH DIAMETER ELLIPSOID

| $Re_{FS} \times 10^6$ | $\alpha$,DEGREES | $C_{M_{FS}} \times 10^2$ | $Re_{IT} \times 10^6$ | $\alpha$,DEGREES | $C_{M_{IT}} \times 10^2$ |
|---|---|---|---|---|---|
| 1.00 | -1.00 | -1.75 | 0.95 | -0.52 | -2.05 |
|  | 0.00 | 0.00 |  | 0.00 | 0.00 |
|  | 0.50 | 0.90 |  | 0.52 | 1.95 |
|  | 1.00 | 1.75 |  | 1.02 | 3.85 |
|  | 1.52 | 2.75 |  | 1.54 | 5.85 |
|  | 2.04 | 3.60 |  | 2.04 | 7.65 |
|  | 2.54 | 4.50 |  | 2.56 | 9.55 |
|  | 3.04 | 5.40 | 0.95 | 3.06 | 11.60 |
|  | 3.54 | 6.15 |  |  |  |
| 1.00 | 4.06 | 7.15 |  |  |  |
| 1.55 | -1.04 | -1.80 | 1.55 | -0.60 | -- |
|  | 0.00 | 0.00 |  | 0.00 | 0.00 |
|  | 0.52 | 0.92 |  | -- | -- |
|  | 1.04 | 1.85 |  | 1.06 | 4.00 |
|  | 1.56 | 2.80 |  | -- | -- |
|  | 2.08 | 3.75 |  | 2.12 | 8.00 |
|  | 2.58 | 4.65 |  | -- | -- |
|  | 3.10 | 5.50 | 1.55 | 3.08 | 11.90 |
|  | 3.60 | 6.30 |  |  |  |
| 1.55 | 4.10 | 7.18 |  |  |  |

TABLE VI (Continued)

| $Re_{FS} \times 10^6$ | $\alpha$, DEGREES | $C_{M_{FS}} \times 10^2$ | $Re_{IT} \times 10^6$ | $\alpha$, DEGREES | $C_{M_{IT}} \times 10^2$ |
|---|---|---|---|---|---|
| 2.05 | -1.06 | -1.95 | 2.00 | -0.56 | -2.00 |
| | 0.00 | 0.00 | | 0.00 | 0.00 |
| | 0.52 | 1.00 | | 0.56 | 2.10 |
| | 1.08 | 1.90 | | 1.10 | 4.10 |
| | 1.58 | 2.88 | | 1.68 | 6.40 |
| | 2.10 | 3.80 | | 2.24 | 8.60 |
| | 2.62 | 4.75 | | 2.82 | 10.80 |
| | 3.16 | 5.65 | | 3.38 | 12.90 |
| | 3.68 | 6.45 | | | |
| 2.05 | 4.20 | 7.35 | 2.00 | | |
| | | | | | |
| 2.30 | -1.08 | 1.95 | 2.25 | -0.60 | -2.20 |
| | 0.00 | 0.00 | | 0.00 | 0.00 |
| | 0.56 | 1.00 | | 0.62 | 2.30 |
| | 1.08 | 2.00 | | 1.20 | 4.60 |
| | 1.60 | 2.90 | | 1.76 | 6.75 |
| | 2.14 | 3.85 | | -- | -- |
| | 2.68 | 4.80 | 2.25 | 2.95 | 11.25 |
| | 3.20 | 5.65 | | | |
| | 3.74 | 6.55 | | | |
| 2.30 | 4.28 | 7.45 | | | |

## DOCUMENT CONTROL DATA - R & D

*(Security classification of title, body of abstract and indexing annotation must be entered when the overall report is classified)*

| 1. ORIGINATING ACTIVITY *(Corporate author)* | 2a. REPORT SECURITY CLASSIFICATION |
|---|---|
| Applied Research Laboratory<br>University Park, Pennsylvania | Unclassified |
| | 2b. GROUP |

**3. REPORT TITLE**

Tunnel Wall Interference for Bodies of Revolution in Non-Steady Motion

**4. DESCRIPTIVE NOTES** *(Type of report and inclusive dates)*

M.S. Thesis, Aerospace Engineering, December 1973

**5. AUTHOR(S)** *(First name, middle initial, last name)*

William R. Hall

| 6. REPORT DATE | 7a. TOTAL NO. OF PAGES | 7b. NO. OF REFS |
|---|---|---|
| August 31, 1973 | 105 | 35 |

| 8a. CONTRACT OR GRANT NO. | 9a. ORIGINATOR'S REPORT NUMBER(S) |
|---|---|
| N00017-73-C-1418 | TM 73-224 |
| b. PROJECT NO. | |
| c. | 9b. OTHER REPORT NO(S) *(Any other numbers that may be assigned this report)* |
| d. | |

**10. DISTRIBUTION STATEMENT**

Approved for Public Release. Distribution unlimited.
Per NAVORD - September 20, 1973

| 11. SUPPLEMENTARY NOTES | 12. SPONSORING MILITARY ACTIVITY |
|---|---|
| | Naval Ordnance Systems Command<br>Department of the Navy |

**13. ABSTRACT**

This thesis considers the problem of determining the effects of tunnel wall interference on the measured values of the stability derivatives for axisymmetric bodies. The tunnel wall interference corrections developed apply equally well to both subsonic wind tunnel or water tunnel testing in tunnels with circular test sections.

A linearized slender body theory is developed which can be used to predict corrections for:

1) the static lift and pitching moment derivatives, $C_{L_\alpha}$ and $C_{M_\alpha}$

2) the rotary damping derivatives, $C_{L_q}$ and $C_{M_q}$

3) the "Add Mass" derivatives, $C_{L_{\dot\alpha}}$ and $C_{M_{\dot\alpha}}$

4) the "accession-to-inertia" derivatives, $C_{L_{\dot q}}$ and $C_{M_{\dot q}}$.

Limited evaluation of the developed theory is presented in the form of static pitching moment tests of three ellipsoids-of-revolution. In addition, comparison is made with two alternative theories developed by Peirce[1] and Goodman.[2]

| 14. KEY WORDS | LINK A | | LINK B | | LINK C | |
|---|---|---|---|---|---|---|
| | ROLE | WT | ROLE | WT | ROLE | WT |
| ACCESSION-TO-INERTIA DERIVATIVES | 8 | | | | | |
| ADD-MASS DERIVATIVES | 8 | | | | | |
| BODY OF REVOLUTION | 8 | | | | | |
| CORRECTIONS | 8 | | | | | |
| PITCHING MOMENTS DERIVATIVES | 8 | | | | | |
| ROTARY DAMPING DERIVATIVES | 8 | | | | | |
| SLENDER BODY THEORY | 8 | | | | | |
| STATIC LIFT DERIVATIVES | 8 | | | | | |
| TUNNEL WALL INTERFERENCE | 8 | | | | | |

DISTRIBUTION

Commander (ORD 632)                  Copies 1 and 2
Naval Ordnance Systems Command
Department of the Navy
Washington, D. C.  20360


Commander (ORD 34B)                  Copies 3 and 4
Naval Ordnance Systems Command
Department of the Navy
Washington, D. C.  20360


Defense Documentation Center         Copies 5 through 16
5010 Duke Street
Cameron Station
Alexandria, Virginia  22314

Via:  Commander (ORD 632)
      Naval Ordnance Systems Command
      Department of the Navy
      Washington, D. C.  20360